Dissertation

EVALUATION OF SPECTRAL-DOMAIN OPTICAL COHERENCE TOMOGRAPHY FOR ANALYSIS OF PROGRESSION OF ATROPHY SECONDARY TO STARGARDT DISEASE TYP IV

submitted by

Dr. med. univ.

Manuel Großpötzl

for the Academic Degree of

Doctor of Medical Science

(Dr. scient. med.)

at the

Medical University of Graz

Department of Ophthalmology

under the supervision of

Priv. Doz. Dr. Rupert Wolfgang Strauß

2024

Declaration

“I hereby declare that this thesis is my own original work and that I have fully acknowledged by name all of those individuals and organisations that have contributed to the research for this thesis. Due acknowledgement has been made in the text to all other material used. Throughout this thesis and in all related publications I followed the “Guidelines of the Medical University of Graz on Good Scientific Practice“.

Graz, 21.03.2024 Manuel Großpötzl

Acknowledgements

Doctoral student Dr. Manuel Großpötzl was enrolled in the Doctoral School of Molecular Medicine and Inflammation

An erster Stelle bedanke ich mich bei Priv. Doz. Dr. Rupert Wolfgang Strauß für die fachliche und freundschaftliche Begleitung und Betreuung während dieses Forschungsprojektes.

Herzlichen Dank an Univ. Prof. Dr. Andreas Wedrich für die Motivation und Unterstützung zur Fertigstellung der Arbeit.

Besonders bedanken möchte ich mich bei meiner Frau, meinem Sohn und meiner Familie, die mir jederzeit mit Rat und Tat zur Seite stehen und mich immer unterstützen.

Disclosure

Parts of this thesis were published in:

Manuel Grosspoetzl[1], Regina Riedl [2], Gernot Schliessleder[1], Zhihong Jewel Hu[3], Michel Michaelides[4,5], SriniVas Sadda[3], David Birch[6], Peter Charbel Issa[7,8,9], Andreas Wedrich[1], Gerald Seidel[1], Hendrik P.N. Scholl[10,11*], Rupert W. Strauss[1,4,5,11,12*] **The Progression of *PROM1*-associated retinal degeneration as determined by spectral-domain optical coherence tomography over a 24-months period.** American Journal of Ophthalmology. [Internet]. 2023 Nov 16 [cited 2023 Nov 18]; Available from: https://www.ajo.com/article/S0002-9394(23)00472-5/fulltext.

[1] Department of Ophthalmology, Medical University Graz, Graz, Austria

[2] Institute for Medical Informatics, Statistics and Documentation, Medical University Graz, Graz, Austria

[3] Doheny Eye Institute, David Geffen School of Medicine at University of California Los Angeles, CA, USA

[4] Moorfields Eye Hospital, NHS Foundation Trust, London, United Kingdom

[5] UCL Institute of Ophthalmology, University College London, London, United Kingdom

[6] Retina Foundation of the Southwest, Dallas, Texas, U.S.A.

[7] Department of Ophthalmology, University of Bonn, Germany

[8] Oxford Eye Hospital, Oxford University Hospitals NHS Foundation Trust, Oxford, United Kingdom

[9] Nuffield Laboratory of Ophthalmology, Department of Clinical Neurosciences, University of Oxford, Oxford, UK

[10] Institute of Molecular and Clinical Ophthalmology Basel, Switzerland

[11] Department of Ophthalmology, University of Basel, Basel, Switzerland

[12] Wilmer Eye Institute, Johns Hopkins University, Baltimore, U.S.A.

The article „The Progression of *PROM1*-associated retinal degeneration as determined by spectral-domain optical coherence tomography over a 24-months period" was published as an open access article distributed under the terms of the Creative Commons CC-BY license by Elsevier, which permits unrestricted use, distribution, and reproduction in any medium, provided the original work is properly cited. In the context of this thesis, when text passages, tables, or figures from this article are reproduced or reused, they will be labeled as (1).

I confirm that all co-authors have explicitly agreed to the use of their published data in this thesis.

Sen. Scientist DI Dr. Regina Riedl of the Institute for Medical Informatics, Statistics and Documentation of the Medical University of Graz assisted with the statistical analysis of this thesis.

Table of Contents

Abbreviations

AAV	Adeno-associated virus
AOSLO	Adaptive optics scanning light ophthalmoscopy
BCVA	Best corrected visual acuity
BEM	Bull´s eye maculopathy
CORD	Cone-rod dystrophy
CRISPR	Clustered regularly interspaced short palindrome repeat
CS	Central subfield
DAF	Decreased autofluorescence
DDAF	Definitely decreased autofluorescence
DIAL	Doheny Image Analysis Laboratory
ELM	External limiting membrane
ELOVL-4	Elongation of very long chain fatty acids-4
ERG	Electroretinogram
ERM	Epiretinal membrane
ETDRS	Early treatment diabetic retinopathy study
EZ	Ellipsoid zone
FA	Fluorescein angiography
FAF	Fundus autofluorescence
ffERG	Full field electroretinogram
mfERG	Multifocal electroretinogram
GCL	Ganglion cell layer
ICGA	Indocyanine green angiography
ILM	Inner limiting membrane
INL	Inner nuclear layer
IPL	Inner plexiform layer
IR	Inner retina
IRD	Inherited retinal disease
IS	Inner segments
IS-OS	Inner segment-outer segment junction

IZ	Interdigitation zone
MCDR2	Macular dystrophy retinal 2
MT	Mean thickness
MZ	Myoid zone
ONL	Outer nuclear layer
OPL	Outer plexiform layer
ORT	Outer retinal tubulation
OS	Outer segments
ProgStar	Progression of *ABCA4*-related Stargardt disease
PROM1	Prominin 1
PRS	Photoreceptor segment layer
QDAF	Questionably decreased autofluorescence
RAD	Relative absolute difference
RC	Reading center
RD	Retinal degeneration
RNFL	Retinal nerve fiber layer
RP41	Retinitis pigmentosa 41
RPE	Retinal pigment epithelium
SD	Standard deviation
SD-OCT	Spectral-domain optical coherence tomography
STGD	Stargardt disease
STGD 1	Stargardt disease type 1
STGD 2	Stargardt disease type 2
STGD 3	Stargardt disease type 3
STGD 4	Stargardt disease type 4
TR	Total retina

Figures

Tables

Abstract in German

Hintergrund: Untersuchung von Veränderungen der Netzhautschichtdicke und der intakten Netzhautfläche bei Patienten mit molekular bestätigter *PROM1*-assoziierter Netzhautdegeneration (RD) über einen Zeitraum von 24 Monaten mittels optischer Kohärenztomographie im Spektralbereich (SD-OCT). Die Dicke der Netzhautschicht und die intakte Fläche sind wichtige Marker für die Gesundheit der Netzhaut, insbesondere bei Erkrankungen wie der Stargardt-Krankheit, und SD-OCT bietet eine präzise Bildgebung, um subtile Veränderungen dieser Parameter zu erkennen.

Design: internationale, multizentrische, prospektiven Fallserienstudie

Methoden: Dreizehn Augen von 13 Patienten mit *PROM1*-assoziierter RD wurden an fünf Standorten untersucht, wobei SD-OCT-Bilder bei Studienbeginn und nach 24 Monaten aufgenommen wurden. Der mittlere Dickenverlust (MT) und die intakte Fläche wurden durch halbautomatische Segmentierung für verschiedene einzelne Netzhautschichten innerhalb des zentralen Unterfelds (CS), des inneren Rings und des äußeren Rings des ETDRS-Rasters (Early Treatment Diabetic Retinopathy Grid) geschätzt: retinales Pigmentepithel (RPE), äußere Segmente (OS), innere Segmente (IS), äußere Kernschicht (ONL), innere Netzhaut (IR) und gesamte Netzhaut (TR). Die Veränderungen der mittleren Dicke und der intakten Fläche der einzelnen Netzhautschichten wurden als jährliche Zunahme der Atrophie und Veränderungen der mittleren Dicke der untersuchten Netzhautschichten und Progressionsmuster analysiert.

Ergebnisse: Sechs männliche und sieben weibliche Patienten mit einem Durchschnittsalter von 38,2±14,2 Jahren zu Studienbeginn und einem Beginn der Symptome im Alter von 30,3±16,3 Jahren (verfügbar für zwölf Patienten) wurden in die Studie aufgenommen. Die mittlere bestkorrigierte Sehschärfe bei Studienbeginn betrug 0,51±0,53 LogMAR. Statistisch signifikante Dickenverluste wurden im RPE und TR im CS und im inneren Ring sowie in der ONL und IS im äußeren Ring beobachtet (alle $p<0,05$). Außerdem wurde eine signifikante Abnahme der intakten Fläche des RPE und der IS im inneren Ring und der ONL im äußeren Ring festgestellt (alle $p<0,05$). Bei der MT und der intakten Fläche der anderen Schichten wurden während des 24-monatigen Beobachtungszeitraums rückläufige Tendenzen beobachtet.

Schlussfolgerungen: Bei Patienten mit *PROM1*-assoziierter RD wurden mittels SD-OCT über einen Zeitraum von 24 Monaten signifikante Dickenverluste in den äußeren Netzhautschichten festgestellt. Derzeit gibt es keine wirksame Behandlung, um die Netzhautatrophie bei Morbus Stargardt aufzuhalten oder rückgängig zu machen. Der Verlust an Dicke und/oder intakter Fläche in diesen Schichten könnte als potenzieller Endpunkt für klinische Studien dienen, die darauf abzielen, das Fortschreiten der *PROM1*-assoziierten RD zu verlangsamen.

Abstract

Purpose: To investigate changes in retinal layer thickness and intact retinal area in patients with molecularly confirmed *PROM1*-associated retinal degeneration (RD) over a 24-month period, utilizing spectral-domain optical coherence tomography (SD-OCT). Retinal layer thickness and intact area are crucial markers of retinal health, particularly in conditions like Stargardt disease, and SD-OCT offers precise imaging for detecting subtle alterations in these parameters.

Design: international, multicenter, prospective case series

Methods: Thirteen eyes from 13 patients affected by *PROM1*-associated RD were enrolled at five sites, with SD-OCT images captured at baseline and after 24 months. Mean thickness (MT) loss and intact area were estimated through semi-automated segmentation for various individual retinal layers within the central subfield (CS), inner ring, and outer ring of the early treatment diabetic retinopathy grid (ETDRS): retinal pigment epithelium (RPE), outer segments (OS), inner segments (IS), outer nuclear layer (ONL), inner retina (IR), and total retina (TR). Changes in mean thickness and intact area of individual retinal layers were analyzed as yearly rate differences and progression patterns.

Results: Six male and seven female patients, with a mean age of 38.2±14.2 years at baseline and symptom onset at 30.3±16.3 years (available for twelve patients) were enrolled. Mean best-corrected visual acuity at baseline was 0.51±0.53 LogMAR. Statistically significant thickness losses were observed in the RPE and TR in the CS and inner ring, and in the ONL and IS in the outer ring (all $p<0.05$). Additionally, a significant decrease in intact area of the RPE and IS was noted in the inner ring, and of the ONL in the outer ring (all $p<0.05$). Trends of decline were observed in MT and intact area of the other layers over the 24-month observational period.

Conclusions: Significant thickness losses in outer retinal layers were detected by SD-OCT over 24 months in patients with *PROM1*-associated RD. Effective treatments to halt or reverse maculopathy in Stargardt's disease are currently lacking. Loss of thickness and/or intact area in these layers may serve as potential endpoints for clinical trials aiming to slow down the disease progression of *PROM1*-associated RD.

1 Introduction

Stargardt disease (STGD) represents a prevalent form of macular dystrophy among young adults, occurring with a prevalence ranging from 1:8.000 to 1:10.000 (2). Its typical onset is during childhood or early adolescence, typically between the ages of 10 and 15 years. Stargardt disease typically advances gradually, with disease severity being influenced by its onset timing; earlier onset indicates usually a more severe disease course. Best corrected visual acuity (BCVA) in affected individuals generally falls within the range of 20/70 to 20/200 (3).

The initial level of visual acuity serves as a predictive factor for the subsequent rate of visual acuity loss. Eyes with baseline visual acuity worse than 20/25 tend to experience faster visual acuity deterioration. Conversely, for those with baseline visual acuity better than 20/25, no significant visual acuity loss is observed over a period of 2 years. Patients with Stargardt disease type 1 (STGD1) who have foveal involvement of the atrophic lesion tend to lose approximately 3 letters of BCVA per year, indicating that individuals with these attributes are prone to more rapid vision decline (4). On the other hand, individuals with STGD1 exhibiting a foveal-sparing phenotype often maintain good visual acuity over an extended duration (5,6).

In STGD1, fixation stability may improve over time (7), as the preferred retinal locus shifts towards the parapapillary region while the scotoma expands (8). Visual acuity, especially in cases with poor fixation stability, may improve once fixation becomes stable (4). There is no observed racial predisposition to the disease. Although the progression of Stargardt disease is gradual, individuals ultimately experience severe visual impairment between their fourth and seventh decades of life (9).

STGD1 stands out as one of the most prevalent genetically inherited retinal diseases (IRDs), contributing to approximately 12% of cases of IRD-related blindness (10).

As proposed by Kong et al., while BCVA holds significant importance as a direct measure of visual function associated with participants' daily activities (11) and frequently serves as the primary endpoint in clinical trials for retinal diseases (12), it may not be a practical outcome measure for STGD1 treatment trials lasting for a 2-year duration due to the minimal rate of change observed during this period (4).

Given the relatively slow progression of the disease, there exists a reasonable window for potential treatment interventions and the opportunity to enhance or postpone further

degeneration over an individual's lifetime. Stargardt disease encompasses a spectrum of phenotypic and genotypic variations, with STGD1 being the most prevalent form (13).

1.1 Stargardt Disease type 1 (STGD 1)

Karl Bruno Stargardt, affiliated with the University of Strasbourg, is credited with publishing the initial comprehensive clinical description, complete with fundus drawings, of seven patients from two families in 1909 who were afflicted with STGD1 (14).

Several decades later, Alex E. Krill and Bertha A. Klien documented the presence of delayed dark adaptation in a comparable cohort of patients, whom they referred to as having "flecked retina syndrome". They conducted the first histopathological examination of an eye from a patient in their third decade of life, concluding that the primary anomaly associated with this condition resides within the retinal pigment epithelium (RPE) (15).

In 1975, Francois confirmed the interconnection among these disorders, identifying characteristic heritable, clinical, and electrophysiological features (16). While recognized as a distinct disease entity, Gerald Fishman, from the Illinois Eye and Ear Infirmary in Chicago, discerned variations in clinical presentation and, consequently, introduced a four-tier classification system (17) that continues to exert a significant influence on ophthalmologists worldwide.

Based on his investigation of fundoscopic and electrophysiological findings in 38 patients, Fishman categorized the severity of STGD1 into the following stages:

- Stage 1: This stage is characterized by localized central macular lesions, which exhibit a spectrum ranging from irregular pigmentary mottling to well-defined lesions displaying RPE atrophy. These lesions typically manifest a distinctive visual appearance, often described as "beaten-bronze" or resembling "snail-slime." These lesions are found beneath central or paracentral scotomas.
- Stage 2: marked by the presence of yellow flecks on the fundus, with some of these flecks potentially undergoing resorption. These flecks extend beyond a distance of one disc diameter from the fovea, encompassing regions that extend beyond the vascular arcades and areas located nasal to the optic disc.
- Stage 3: is characterized by the widespread resorption of flecks and the occurrence of choriocapillaris atrophy within the macula.
- Stage 4: This stage is distinguished by extensive choriocapillaris atrophy throughout the posterior pole of the eye, leading to a moderate to severe limitation of peripheral visual fields (17) (Figure 1, Figure 2).

Approximately two-thirds of patients diagnosed at stage 1 of STGD1 maintain their status in this stage during a follow-up period spanning 5.4 years. For patients initially diagnosed in stages 2 and 3, it has been reported that roughly 70% to 86% of cases, respectively, exhibit stability over follow-up periods of 7.2 and 5.3 years (18).

Subsequently, numerous clinical studies have contributed to the expanding knowledge base in this field. However, the "modern era" of our comprehension of STGD1 was ushered in by concurrent advancements in basic scientific research, commencing with the initial characterization of the ABCA4 protein in 1978. This protein was originally referred to as the "rim" protein due to its localization within the rod photoreceptor outer segments and incisures (19). In the mid-1990s, the genetic locus was mapped to 1p13 (20,21), and in 1997, the gene was ultimately cloned (2).

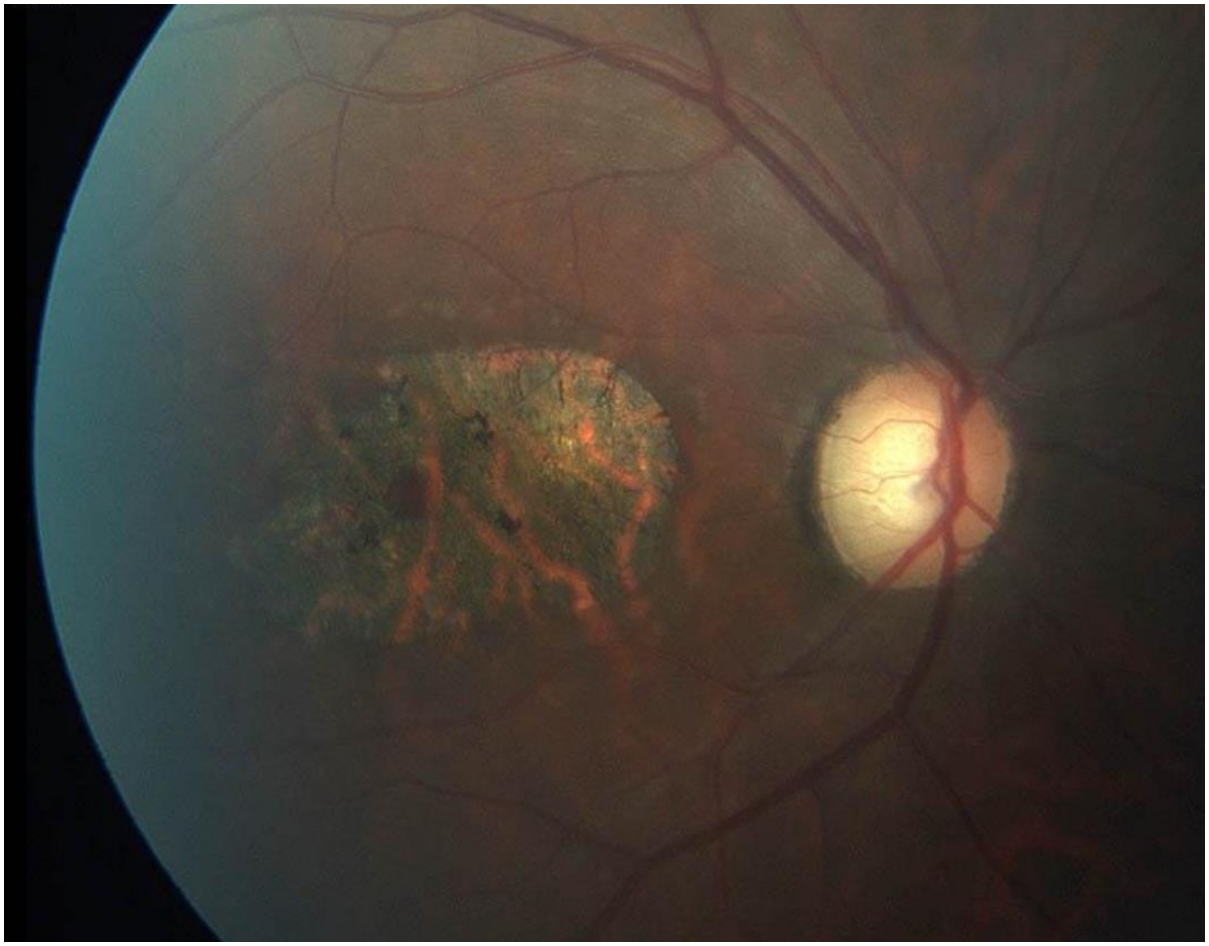

Figure 1: Fundus image of the posterior pole of a right eye with Stargardt's disease type 1 showing marked chorioretinal atrophy and pigmentary clumps.

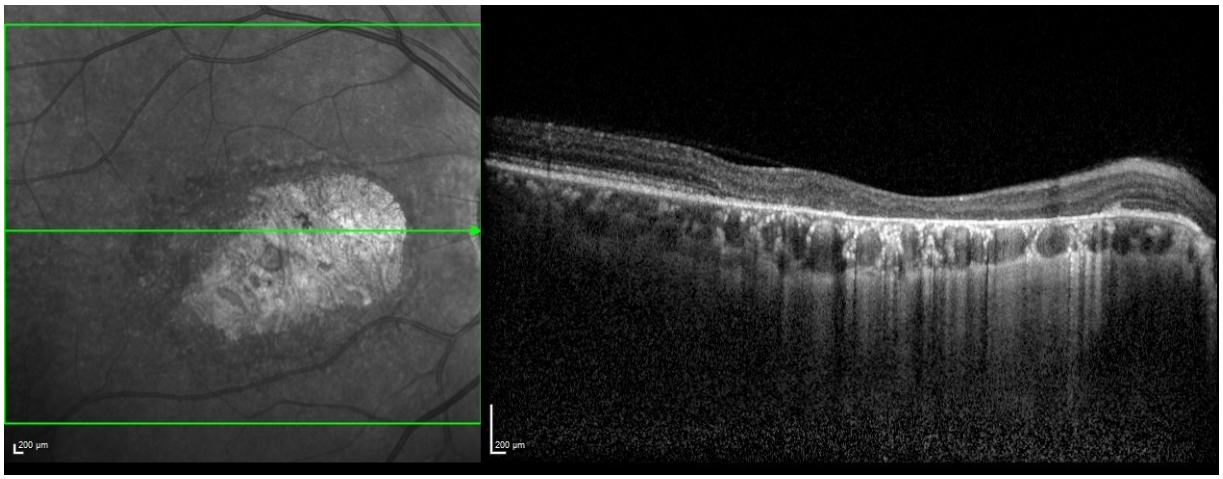

Figure 2: Spectral domain optical coherence tomography of a right eye of the same patient as seen in figure 1 with circumscribed atrophy of the outer retinal layers.

A mutation in the *ABCA4* gene (located at cytogenetic location 1p22.1) results in a malfunctioning ATP-binding cassette protein transporter within the outer segments of the rods. This transporter plays a crucial role in expelling harmful substances generated after phototransduction from the photoreceptors. The accumulation of these substances, primarily lipofuscin, leads to the demise of photoreceptors and adjacent cells. A slight reduction in *ABCA4* activity gives rise to Stargardt's disease, accounting for approximately 95% of cases. With a moderate alteration, a phenotype akin to cone-rod dystrophy emerges, encompassing 30-50% of cases. Complete loss of *ABCA4* activity results in a phenotype reminiscent of retinitis pigmentosa, affecting about 8% of cases and characterized by the complete loss of both cones and rods (3). Notably, a quarter of childhood-onset STGD1 cases do not exhibit any retinal lesions upon initial presentation (22).

1.2 Stargardt Disease type 2 (STGD2)

A significant revelation in the realm of genetic research and hereditary eye disorders occurred when it was determined that Stargardt disease type 2 (STGD2) and Stargardt disease type 3 (STGD3) were, in fact, attributable to the same gene. This pivotal discovery led to the subsequent discontinuation of the term STGD2 in 2005.

Before this unification, STGD2 and STGD3 were regarded as distinct classifications, potentially leading to some confusion within the scientific and medical community. The recognition that they shared a common genetic basis not only simplified the categorization of Stargardt disease but also had profound implications for our understanding of its underlying genetic mechanisms.

The merging of STGD2 and STGD3 into a single entity highlighted the genetic complexity of Stargardt disease and emphasized the significance of accurate and updated nomenclature in the field of genetic medicine. This harmonization allowed for a more cohesive approach to research, diagnostics, and potential therapeutic interventions related to this condition.

This pivotal moment in the history of Stargardt disease research serves as a testament to the dynamic nature of genetic science, where ongoing discoveries and refinements continually shape our comprehension of hereditary disorders and, in turn, pave the way for more effective approaches to diagnosis and treatment.

1.3 Stargardt Disease type 3 (STGD 3)

In the year 2001, a significant breakthrough in the understanding of STGD3 emerged when two separate research teams, working independently, uncovered a critical genetic anomaly. Specifically, they identified a 5-base pair deletion (797–801delAACTT) located within exon 6 of the *Elongation of Very Long chain fatty acids-4* (*ELOVL4*) gene. This discovery provided a vital link between this genetic mutation and the onset of STGD3 pathology (23,24). The *ELOVL4* gene encodes a protein that holds an important role in the biosynthesis of a specific class of lipids known as very long-chain fatty acids. These lipids play crucial roles in various cellular processes. However, when mutations occur in the *ELOVL4* gene, they lead to the aggregation of the ELOVL4 protein within cells, disrupting its normal function. Over time, this disruption culminates in cell death, contributing to the pathogenesis of STGD3. The *ELOVL4* gene is located at the cytogenetic region 6q14.1, which serves as a precise chromosomal address for its genetic location (3). Individuals affected by STGD3 typically experience the early onset of central vision loss, which progressively deteriorates as the disease advances. The degeneration initially affects the fovea. However, over time, this degeneration extends to involve the peripheral retina, further impairing an individual's visual capacity (24).

1.4 Stargardt Disease type 4 (STGD 4)

Stargardt disease type 4 (STGD4) stems from disease-causing variants located within the *PROM1* gene, situated on chromosome 4 (25). *PROM1* encodes a 5-transmembrane domain protein characterized by two extensive, highly glycosylated extracellular loops and a cytoplasmic tail (26). While it is known to be associated with plasma membrane protrusions (27), its precise function and specific molecular interactions remain largely unresolved. *PROM1* is expressed in various tissues (28,29). These *PROM1* variants can be inherited as either autosomal dominant or autosomal recessive traits (29,30). A case series encompassing five unrelated families, as reported by Michaelides and colleagues, has revealed diverse phenotypes, including macular dystrophy retinal 2 (MCDR2), autosomal dominant bull's eye macular dystrophy (BEM), STGD4, retinitis pigmentosa 41 (RP41), severe retinitis pigmentosa with macular degeneration, and cone-rod dystrophy (CORD) (31).

Within the outer segments (OS) of the retina, the *PROM1* gene (*PROM1*; also known as *CD133* and *AC133*) encodes the prominin 1 protein, which plays a critical role in the organization and formation of photoreceptor disks (25,29,30). Consequently, a faulty form of the PROM1 protein

is produced, which remains localized in the myoid region of photoreceptors and is unable to migrate to the OS region where disk formation occurs. This disruption affects the growth and arrangement of photoreceptor disks, particularly in the region where most electrochemical signals in response to light are generated, encompassing the visual cycle-phototransduction process. A missense mutation that leads to the expression of a mutant *PROM1* is associated with three forms of autosomal-dominant retinal dystrophies(30).

In transgenic mice carrying the mutant *PROM1*, the protein is mislocalized, leading to defects in both rod and cone photoreceptor cells. These mice exhibit reduced electroretinogram (ERG) responses, and photoreceptor cell loss occurs in a manner that correlates with the expression level of the mutant *PROM1*. Notably, the mutation in *PROM1* disrupts its interaction with *PCDH21* and actin. Prior to degeneration, aberrations are observed in the disks of photoreceptor OS, providing strong evidence for *PROM1's* role in the morphogenesis of new disk membranes (30).

It is noteworthy that, despite a previous study demonstrating the expression of the *R373C* mutated human *PROM1* gene under the control of the rhodopsin promoter, thus localizing its expression to rod photoreceptors, clinical features of *PROM-1* related retinopathies include cone photoreceptor impairment (30).

Prior investigations have associated mutations in the *PROM1* gene with autosomal-recessive retinitis pigmentosa in pedigrees (28,32). These mutations predominantly affect rod photoreceptors and peripheral vision. These mutations are characterized by frameshift mutations, leading to the premature termination of protein synthesis and the resulting truncation of the encoded protein, most likely representing null mutations. Experimental transfection studies revealed that the truncated protein undergoes rapid degradation, with a small fraction being detected within the endoplasmic reticulum and no presence on the cell surface. Consequently, the degeneration observed in these patients is believed to result from the loss of *PROM1* function (32). Conversely, the *R373C* mutation leads to the production of a stable mutant protein, resulting in dominant macular degeneration primarily affecting cone photoreceptors and central vision. The *R373C* mutant PROM1 protein was observed to be mislocalized, causing the misplacement of both the wild-type PROM1 protein and at least one other crucial protein, PCDH21 (30).

The recessive form of the disease is linked with early-onset, severe panretinal degeneration and with early central vision loss, whereas the dominant disease typically manifests as late-onset

dystrophy predominantly affecting the macula (33) (Figure 3). An analysis of PROM1 genetic variations has shown that sequence variations are distributed across the entire protein, without significant clustering in a domain-dependent manner. This observation suggests that the entire protein plays a critical role in its function. The severe homozygous recessive phenotype is likely associated with null variants that completely disrupt the function of alleles, leading to the absence of *PROM1* (33).

Elucidating the mechanisms underlying *PROM1* degeneration holds significant implications for the development of potential therapeutic approaches. For instance, subretinal delivery of an adeno-associated viral vector carrying the *PROM1* gene (2.5 kilobase pairs) to photoreceptors in the early stages of recessive dystrophy could replace the null protein and potentially rescue the phenotype. However, in the case of the dominant variant, an initial silencing step, such as RNA silencing using a mirtron (34), would be required, followed by a gene replacement therapy involving the wild-type protein, referred to as block-and-replace therapy. In more advanced stages of the disease, where irreversible damage to photoreceptors has occurred, the restoration of vision through optogenetic treatment (35) may serve as an alternative therapeutic approach. Furthermore, the widespread expression of *PROM1* facilitates the development of in vitro models for *PROM1* gene therapy and related functional assays (33).

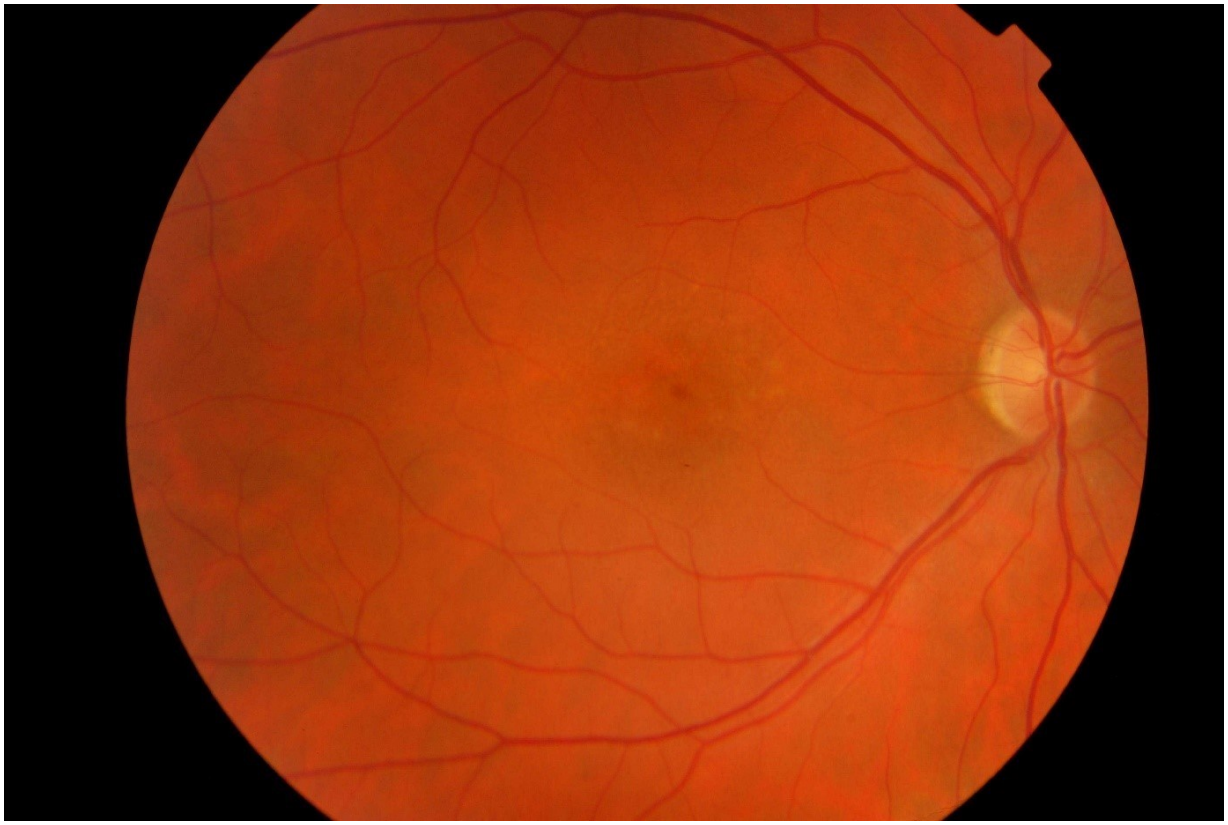

Figure 3: Fundus image of the posterior pole of a right eye with Stargardt's disease type 4, with delicate annular pigmentary shift around the fovea.

1.4.1 Interaction of *PROM1* with *PCDH21*

Rattner et al. (36,37) reported the existence of a photoreceptor cadherin known as *PCDH21*, which, akin to *PROM1*, localizes to the developing disks of both rod and cone outer segments (OS). Remarkably, similar to *PROM1 R373C* mutant mice, *PCDH21*–/– mice exhibit disarrayed photoreceptor membrane disks within their OS, accompanied by photoreceptor degeneration. These findings lend support to the notion of a functional interaction between *PROM1* and *PCDH21*. Evidence for this interaction emerged from the co-localization of *PROM1* and *PCDH21* at the base of OS, as well as the successful co-immunoprecipitation of full-length *PCDH21* with *PROM1*. Further support for this interaction was gleaned from an analysis of molecular abnormalities in *R373C PROM1* transgenic mice. *PCDH21* exhibited a coinciding mislocalization pattern with the *R373C* mutant protein within photoreceptors. Immunoblot analysis additionally revealed a substantial reduction in cleaved *PCDH21* levels in retinal lysates from *R373C* mutant mice. Given that the loss of *PCDH21* leads to retinal degeneration (36), it is conceivable that the dominant impact of the *R373C PROM1* mutation

on retinal degeneration may arise from the impairment of *PCDH21* function. Since both *PROM1* and *PCDH21* are found on nascent disks, it is plausible that their interaction occurs within the same membrane or between adjacent membranes of two nascent disks. In the latter scenario, they might play a role in maintaining the spacing between neighbouring disk membranes (30).

1.5 Phenotype Transmission

The field of genetics owes its origins to the meticulous observations made by a 19th-century monk named Gregor Mendel in the confines of a monastery garden. Mendel's groundbreaking laws elucidated the mechanisms governing the inheritance of characteristic traits as they pass from one generation to the next, exemplified by traits like the texture of pea skin (wrinkled or smooth) and the colour of pea plant flowers (white, pink, or red). Although the terminology of "genes" would not be introduced until much later, Mendel's laws have endured the test of time and our ever-expanding understanding of biology, with some notable exceptions. Gregor Mendel put forth three fundamental laws to elucidate the inheritance of observable traits that are passed down through generations, as exemplified by characteristics in pea plants. Today, we comprehend that these traits are encoded within our DNA. These seemingly straightforward alterations in an organism's phenotype—the observable trait—can be attributed to changes in our genes (38).

Mendel's monohybrid crosses involving pea plants unveiled patterns of phenotype inheritance that laid the foundation for subsequent clinical investigations, leading to the unravelling of various inheritance patterns within families. The examination of disease transmission in extensive family pedigrees has identified five primary patterns, which are categorized based on whether the mode of inheritance is dominant or recessive and whether the phenotype is transmitted via autosomal or sex chromosomes. In cases where a disease is inherited in an autosomal dominant manner, the presence of a single disease-causing allele on autosomal chromosomes is adequate to result in the affected status. Conversely, autosomal recessive inherited disorders necessitate the presence of two disease-causing alleles on autosomes for the disease to manifest (39).

As we delve into the exploration of *PROM1* gene variants, our understanding of how these genetic variations manifest as observable traits and phenotypes remains far from complete. Furthermore, the complex molecular mechanisms governing these sequence variations and their

effects on the functionality of the associated protein are still a largely unexplored domain. Additionally, the question of whether *PROM1* primarily influences the characteristics of cone or rod photoreceptors, and the puzzle of how variants within the same gene can result in differing genetic traits, some exhibiting recessive patterns while others display dominant expression, remain enigmatic (33).

1.6 Clinical Manifestation

The clinical presentation of Stargardt's disease exhibits a range of characteristics, with the most common initial symptom being a decline in visual acuity. Clinical evidence often includes macular degeneration, characterized by alterations in the retinal pigment epithelium (RPE) and the presence of retinal flecks. Fundus fluorescein angiography can reveal the "dark choroid" sign and hyperfluorescent macular lesions. Full-field electroretinograms (ERGs) typically demonstrate signs of generalized dysfunction in rod photoreceptors and/or rod-cone dysfunction (31).

Utilizing multimodal imaging techniques is crucial for the early detection of subtle changes in the outer retinal layers that precede the development of a "beaten bronze" appearance in the macula. It is also essential for identifying the accumulation of lipofuscin in the RPE before the formation of subretinal flecks. Detecting preclinical lesions holds particular significance in the screening of younger, asymptomatic siblings of a child with confirmed STGD. Additionally, performing multimodal imaging in both parents is necessary to identify cases of asymptomatic late-onset STGD that may mimic age-related macular degeneration (AMD) or a pattern dystrophy with pseudodominant inheritance (40,41).

1.6.1 Early Perturbations in young patients

The existing body of research suggests that in young patients, the decline in visual function may precede the observable fundus abnormalities during clinical examinations. However, it's worth noting that asymptomatic cases, particularly those with foveal sparing, may be incidentally encountered through routine examinations (42,43). In a cohort of 50 young patients with *ABCA4*-associated retinopathy, aged 10 years or younger, Lambertus and colleagues identified ten individuals who exhibited visual function loss in the absence of evident fundus abnormalities at the time of examination. Their findings indicated that the decline in visual acuity could begin as early as three years of age (22). Additionally, cases of impaired colour

vision have been documented in patients with minimal to no discernible fundus changes (44). It is plausible that structural alterations may precede functional losses in these patients.

1.6.2 Fundus Flecks

The augmented accumulation of lipofuscin within the RPE occurs extensively throughout the retina. However, this process can also manifest locally, giving rise to one of the most recognizable characteristics of *ABCA4*-associated retinopathy—retinal flecks. These flecks are particularly prominent in short-wavelength autofluorescence (SW-AF) imaging, appearing as intensely fluorescent foci distributed across the macula or extending more extensively across the posterior pole, especially in advanced disease stages (45,46).

Histopathological examinations have previously attributed the presence of these flecks to engorged RPE cells, stacked aggregations of RPE cells, or remnants of dying RPE cells (47). However, more recent insights from Sparrow et al. suggest that these flecks may actually represent extracellular accumulations of un-phagocytized OS. This proposition is based on longitudinal observations of their structural characteristics using spectral-domain optical coherence tomography (SD-OCT) and their autofluorescence patterns under SW-AF and near-infrared autofluorescence (near-infrared-AF) imaging over time (48).

The ubiquity of flecks in *ABCA4*-associated retinopathy renders them a valuable diagnostic tool in clinical settings. However, the inherent variability in their size and morphology, as well as their irregular distribution across the fundus and spatial changes over time, may obscure critical information concerning the disease's origin and prognosis. Flecks are generally considered indicative of disease severity, as they emerge along both the central and peripheral axes of the retina in *ABCA4*-associated retinopathy (9).

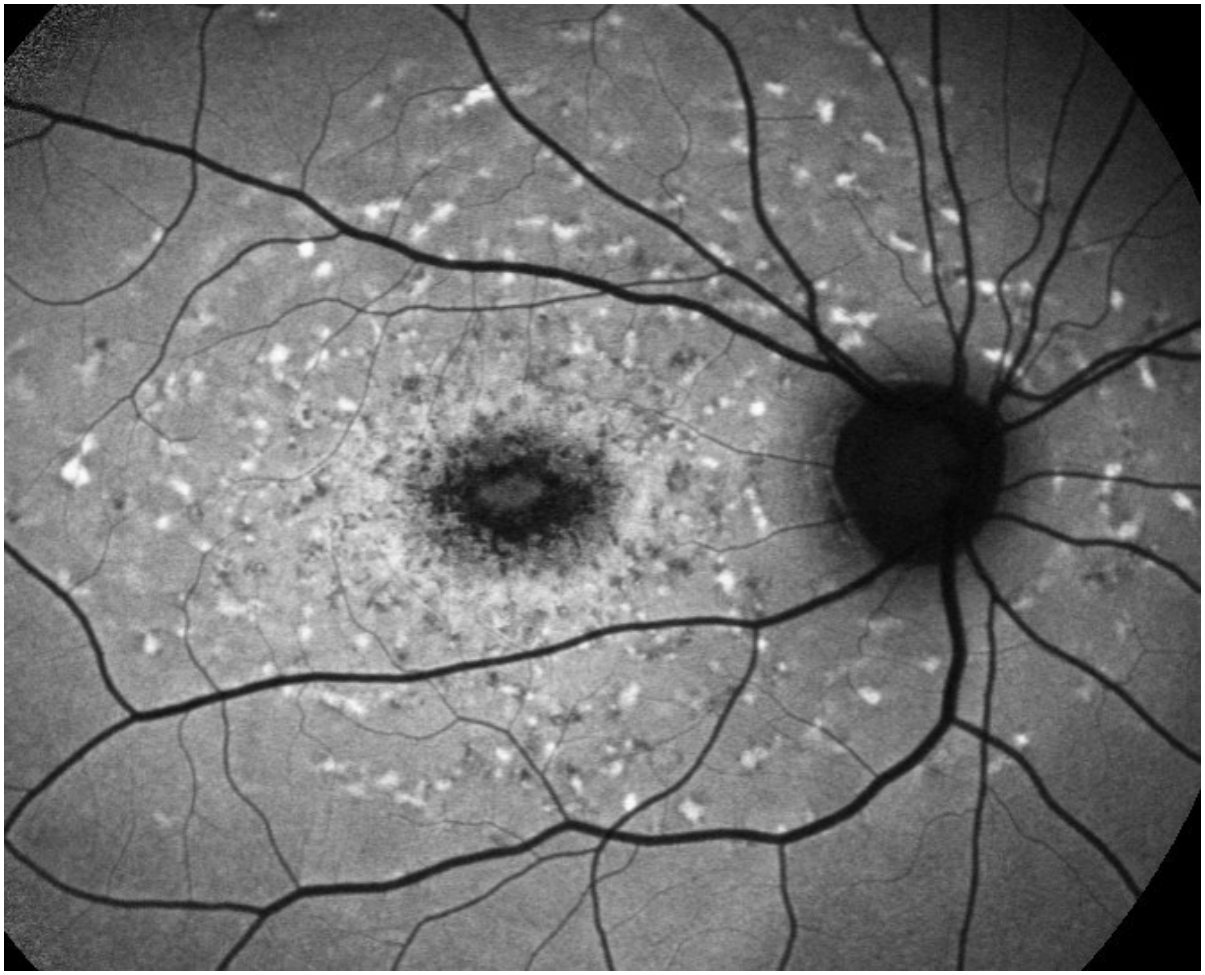

Figure 4: Fundus autofluorescence image of the posterior pole of a right eye of a patient with morbus stargardt type 1 showing central questionable decreased autofluorescence (QDAF) with surrounding annular definitely decreased hypofluorescence (DDAF) followed by annular QDAF and annular hyperfluorescence. Patchy hyper and partially hypofluorescent lesions are seen throughout the area of the posterior pole and around the optic disc.

1.6.3 Bull´s Eye Maculopathy

The term "bull's-eye maculopathy" was initially coined in the context of describing chloroquine retinopathy. Subsequently, bull's-eye lesions have been identified in various conditions, including cone dystrophy, cone-rod dystrophy, rod-cone dystrophy, and several forms of macular dystrophy, such as benign concentric annular macular dystrophy, among others. However, the precise underlying mechanisms leading to the development of bull's-eye maculopathy remain poorly understood. Characteristic features of bull's-eye maculopathy include a ring-shaped disruption of the RPE, with the central area being spared initially. This pattern is attributed to the accumulation of lipofuscin in the RPE, which is typically most

concentrated at the posterior pole in healthy individuals, creating a depression in the fovea (Figure 5 and Figure 6). However, as the disease progresses, it often extends to affect the central region that was initially spared (49).

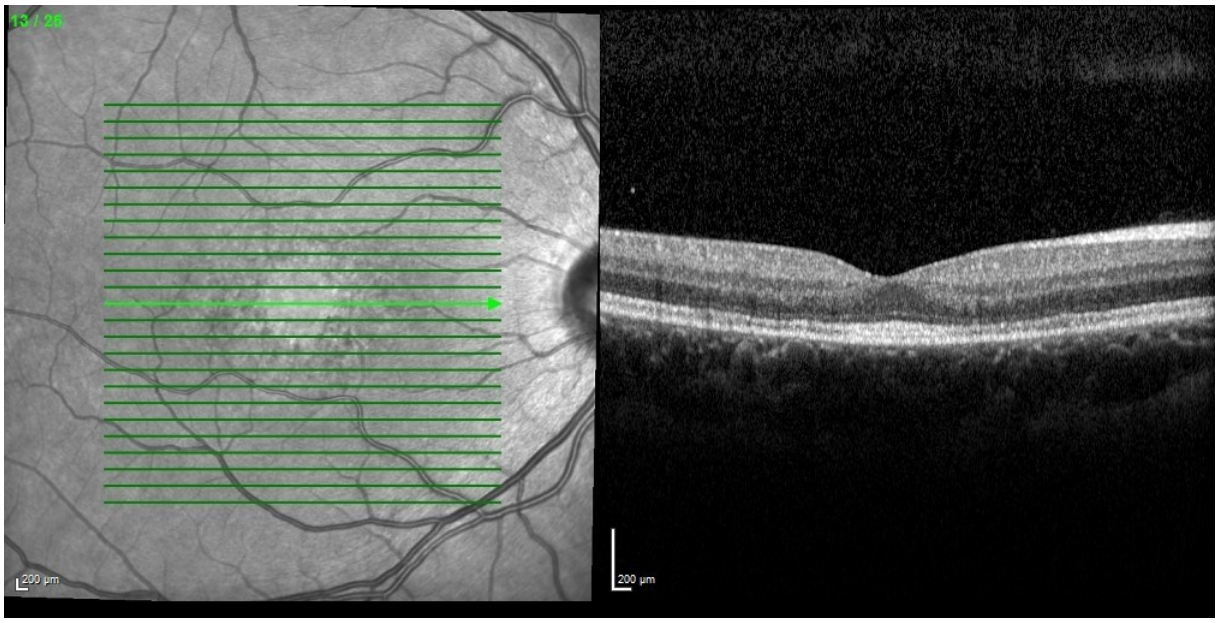

Figure 5: Spectral domain optical coherence image (SD-OCT) of a right eye with morbus stargardt type 4 with preserved central retinal layers. Around the center, loosening and interruption of ellipsoid zone in the sense of bull's eye maculopathy is visible.

1.6.4 Peripapillary Sparing

One of the most noteworthy features within the triad of characteristics is the observation that the tissue proximal to the optic nerve remains unaffected by disease changes in *ABCA4*-associated retinopathy (8). Similar manifestations have been reported in other diseases, notably *PRPH2*- and *ROM1*-associated pattern dystrophy, and *RDH12*-associated Leber congenital amaurosis, although such sparing is not as consistently observed as in *ABCA4*-associated retinopathy. In the case of *ABCA4*-associated retinopathy, the preservation of this region, both structurally and functionally, often persists, but it tends to be progressively lost in later disease stages. Nevertheless, the underlying cause of this phenomenon remains unknown (9).

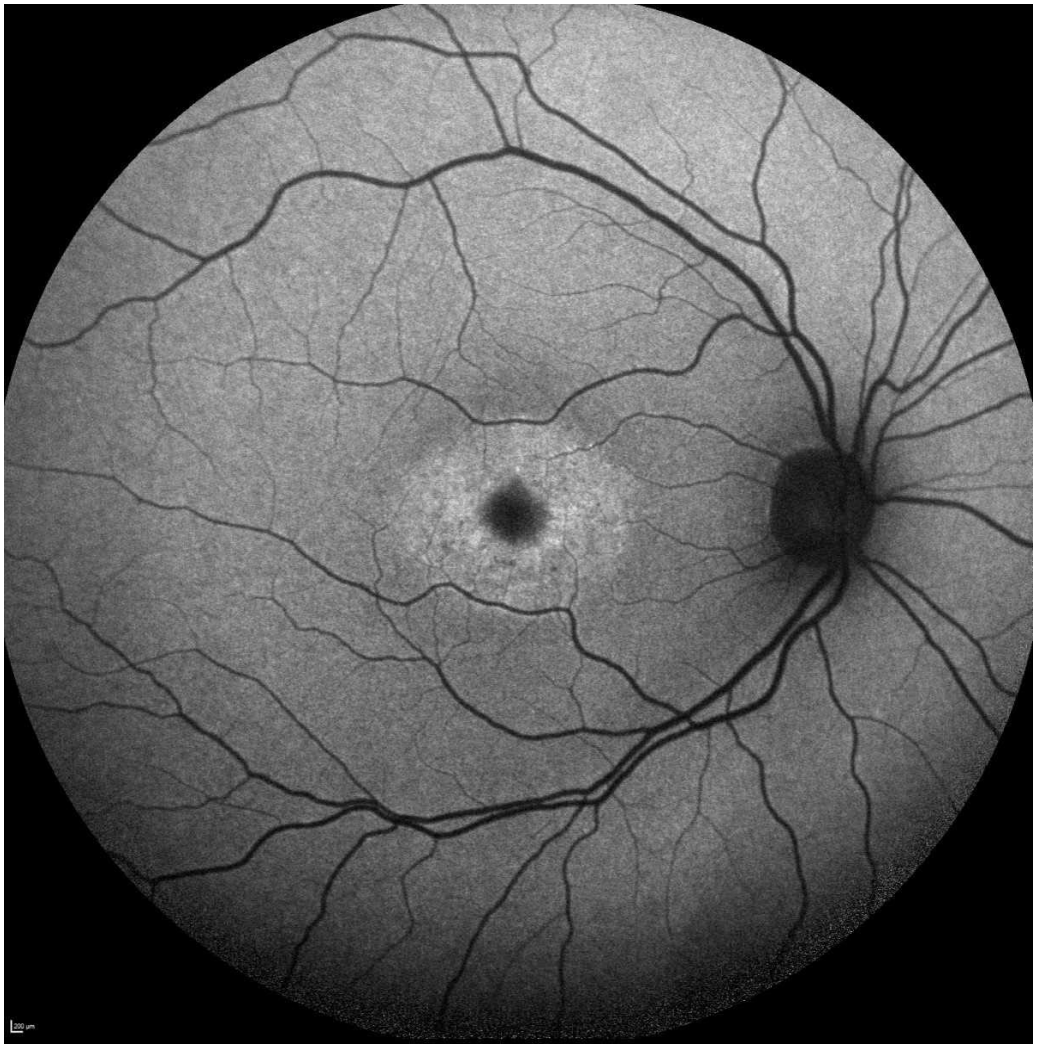

Figure 6: Fundus autofluorescence image of the same patient as in figure 5 with hyperautofluorescence centrally in the sense of bull´s eye maculopathy is visible.

1.7 The Retina

The retina, a delicate multi-layered structure primarily composed of neuronal cells derived from the ectoderm, serves as a central component in the visual system. Much like the role of photographic film in a camera, the retina is responsible for capturing, modulating, and transmitting visual stimuli from the external environment to the optic nerve and, ultimately, to the visual cortex of the brain. The effective transmission of visual signals heavily depends on the specialized anatomical features of the retina. Various factors or injuries to the retina can initiate pathological processes that disrupt this intricate structure, leading to the onset of retinal diseases. The thickness of the retina measures roughly 0.4 mm at the border near the optic nerve head, gradually tapering toward the periphery until it reaches an approximate thickness of 0.14

mm at the ora serrata. Within the clinical macula, a circular region measuring 1.5 mm in the neural retina, the thickness varies from 0.35 mm at its periphery to a gradual slope down to 0.18 mm at the foveola. In this specific area, cone photoreceptors exhibit a high density, with approximately 4,000 to 5,000 cones per square millimeter in the macula and an impressive 15,000 cones per square millimeter in the fovea. Rod photoreceptors, on the other hand, reach their peak density at a distance of 20° from the fixation point. Foveal cones establish one-to-one connections with up to 5 ganglion cells, while, on average, a single ganglion cell typically connects with about 130 different photoreceptors. (50–52).
Recent advancements in imaging modalities have led to changes in the nomenclature of individual retinal layers.

When classified by spectral-domain optical coherence tomography (SD-OCT) in accordance with histological nomenclature, the retina can be divided into layers in the following sequence, progressing from inner to outer layers, as per the International Nomenclature for Optical Coherence Tomography (IN*OCT) consensus study group (53):

- Internal limiting membrane (ILM)
- Retinal nerve fiber layer (RNFL)
- Ganglion cell layer (GCL)
- Inner plexiform layer (IPL)
- Inner nuclear layer (INL)
- Outer plexiform layer (OPL)
- Outer nuclear layer (ONL)
- External limiting membrane (ELM)
- Myoid zone (MZ): myoid portion of inner segments of photoreceptors
- Ellipsoid zone (EZ): interface between inner and outer segments of photoreceptor segments - containing the inner and outer segment junction
- Interdigitation zone: tight junction complexes between RPE cells
- Retinal pigment epithelium (RPE)

Light must traverse these many layers before initiating signal transduction in the rods and cones.

1.8 Clinical Outcome Measures

The selection of appropriate clinical outcome measures for STGD should be based on a thorough understanding of the underlying factors influencing disease progression. The natural course of STGD encompasses multiple trajectories primarily influenced by an individual's genotype. Effective outcome measures should be applicable to a broad spectrum of patients while also considering their individual variations.

Visual function impairment represents the primary symptom in all inherited retinal diseases. Therefore, it is crucial to develop effective methods for monitoring this impairment over time, as it is essential for assessing disease progression and response to treatments. In addition to clinical evaluations, diagnostic tools such as fluorescein angiography, fundus autofluorescence (FAF), spectral domain optical coherence tomography (SD-OCT), and electroretinography (ERG) are employed for diagnosis and characterizing the clinical phenotype. Some of the findings from these imaging techniques may also carry prognostic implications.

1.8.1 Fluorescein Angiography

The majority of individuals with *ABCA4*-associated retinopathy typically display a localized and spatially uniform increase in RPE lipofuscin levels due to *ABCA4* dysfunction (54). This heightened RPE lipofuscin often imparts a vermilion hue to the fundus when observed under white light imaging and can hinder the fluorescence emanating from the underlying choroid during fluorescein angiograms (FA), resulting in the distinctive "dark" or "silent" choroid appearance, which is observed in up to 62% of patients (9) (Figure *7*). Despite the historical usefulness of FA, its role in assessing STGD has become increasingly limited, as it is no longer routinely performed in favour of newer, less invasive imaging techniques.

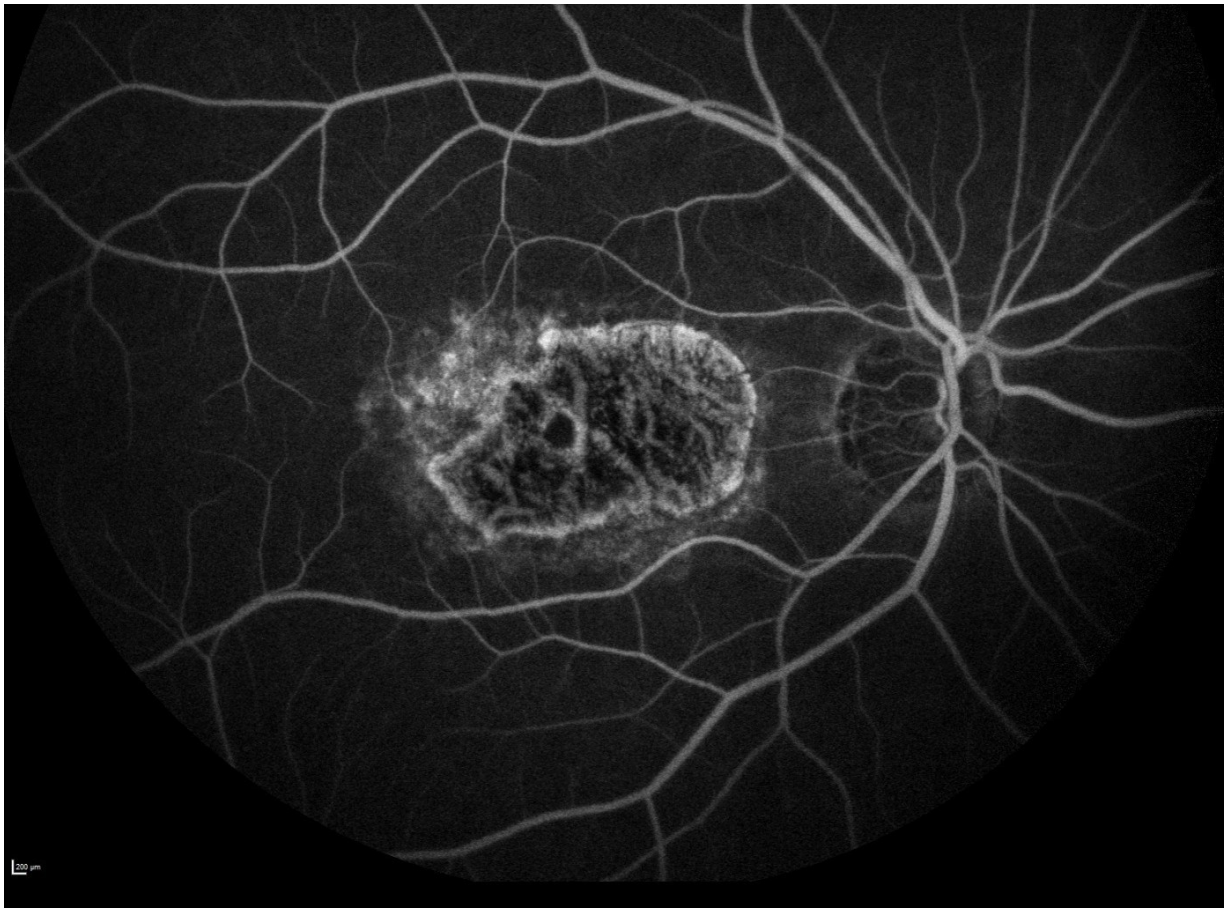

Figure 7: Fluorescence angiography image of a right eye with Stargardt's disease showing an oval window defect with translucency of the choroidal vessels centrally, tender hyperfluorescence around the window defect and the classic image of dark choroid.

1.8.2 Spectral-Domain Optical Coherence Tomography (SD-OCT)

In recent years, the importance of multimodal imaging in the study of chorioretinal diseases has increased significantly, providing a more comprehensive understanding of the manifestations and pathogenesis of various conditions.

SD-OCT is an imaging technique capable of capturing structural changes by offering quasi-histological sections of the retina and choroid in vivo. The imaging of the choroid using SD-OCT has become increasingly popular, particularly with the introduction of enhanced depth imaging. This technique involves positioning the zero-phase delay line at the choroidal side of the image frame, effectively inverting the image (55).

SD-OCT employs the combination of multiple images acquired from the same location, effectively filtering out random speckle noise while retaining data common to all the images. This process preserves information reflected from physical structures, while reducing image

noise, resulting in higher-quality images with finer details. The device is equipped with an eye tracking system that simultaneously captures images of the eye using two beams of light. One beam creates a retina image and maps more than 1,000 points to monitor eye movements. Using this mapped image as a reference, the second beam is directed precisely to the desired location, compensating for blinks or saccadic eye movements. The eye tracking system minimizes the artifacts caused by eye motion and ensures accurate correlations between SD-OCT and fundus images, eliminating the need for post-processing. Additionally, the system reduces operator variability in follow-up scans by employing an auto rescan feature. This feature locks onto a specific retinal location and relocates it during subsequent examinations, enhancing the monitoring of disease progression and treatment decisions. This adds precision to the analysis of retinal thickness changes and FAF. Moreover, the device has been the subject of several studies that have provided normative and disease-related data, serving as valuable reference material (56–60).

SD-OCT in patients with Stargardt´s disease type 1

One of the earliest structural changes observed in patients with STGD1 was identified in the ONL. Furthermore, SD-OCT images revealed a distinct increase in reflectivity extending inward from the ELM. This change in thickness is most pronounced at the foveola and appears to decrease gradually as eccentricity increased, eventually becoming imperceptible at the outer boundary of the foveal avascular zone, as defined by near-infrared reflectance images. Notably, the reflectivity within the innermost vitreal portion of the ONL, where Henle fibers are located, remains unaffected throughout this process (42). This atypical SD-OCT abnormality has been termed "ELM thickening" due to the increased reflectivity that seems to connect with the ELM (61). The ELM represents the adherent junctions between Müller cells and either other Müller cells or the inner segments of photoreceptors. It appears unlikely that such thickening of this structure would occur as the initial sign of STGD1 (62) An alternative hypothesis, proposed by Khan et al., suggests that these identified changes may result from pathological disruptions within the outer lamella of the ONL, particularly affecting cone photoreceptors (42). Within the ONL, cone photoreceptor nuclei are known to have a specific spatial distribution, with the highest density and tightest packing observed at the fovea, gradually becoming less densely packed as they approach the ELM in the perifoveal retina. In contrast, rod nuclei are believed to have a less spatially restricted distribution, spanning the entire thickness of the ONL (63).

SD-OCT imaging confirmed the continued presence of the EZ in early disease stages but suggested a qualitative reduction in its intensity. This indicates that, in addition to the changes in the ONL, subtle pathological alterations may affect the outer segments of photoreceptors. Furthermore, increased reflectivity within the ONL appears to be a temporary phenomenon, persisting only as long as the volume of the ONL is preserved. Meanwhile, the line corresponding to the ELM remains unchanged at this stage. (42). Indeed, previous observations have highlighted the robust nature of the ELM, even in patients with advanced disease (43). Sequential imaging provided further insights into the precise sequence of events leading to macular atrophy. When a substantial number of photoreceptor nuclei were lost, SD-OCT documentation indicated a collapse of the inner retinal layers into the ONL (Figure *8*Figure *8*), with this phenomenon appearing to occur primarily at perifoveal locations, initially sparing the foveola (42).

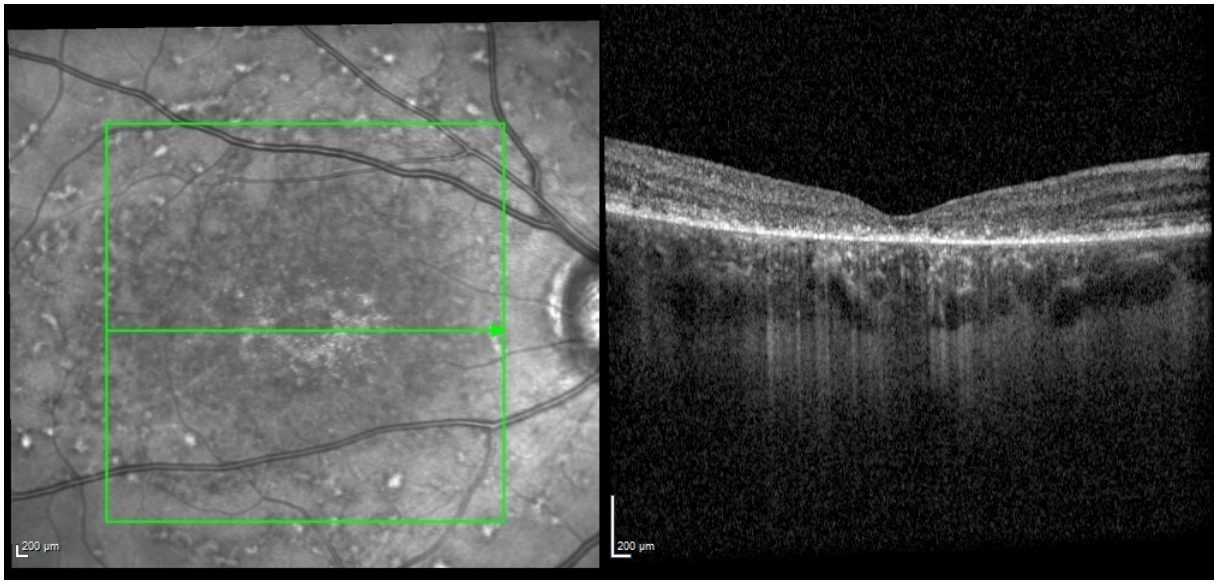

Figure 8: Spectral domain optical coherence tomography of a patient's right eye with morbus stargardt type 1 with central loss of the outer retinal layers.

1.8.3 Fundus Autofluorescence

FAF imaging is a diagnostic method that relies on the detection of naturally occurring fluorophores, primarily located within the photoreceptors and RPE, to create a metabolic profile map of the fundus. This imaging technique, originally introduced for in vivo retinal examination by Delori et al. (64) is based on the fundamental principles of fluorescence. In fluorescence, a molecule absorbs a photon with a specific excitation wavelength, undergoes energy

transformations, and emits a photon with a lower energy level, characterized by a specific emission wavelength. FAF imaging shares similar principles with other imaging modalities such as FA and indocyanine green angiography (ICGA). However, in FAF imaging, the substances being imaged are inherent fluorophores already present within the retinal structures, eliminating the need for systemic dye administration. Given the relatively low natural fluorescence of these substances, the auto fluorescent signals generally require amplification compared to the signals obtained with dyes (65).

FAF imaging serves as a non-invasive method to map the distribution of fluorophores within the RPE (66). In the context of STGD1, the impaired function of the *ABCA4* flippase in both photoreceptors and RPE results in cellular dysfunction. This dysfunction leads to the formation of subretinal clumps consisting of lipofuscin-rich degenerate outer segments, often referred to as "flecks." Over time, these pathological changes can lead to the degeneration of RPE and photoreceptor cells (48).

Hyperautofluorescent and hypoautofluorescent lesions

Hyperautofluorescent lesions represent one of the earliest features observed in FAF, often becoming apparent before they are clinically visible as flecks or can be captured in colour photographs. These lesions exhibit a range of shapes and sizes, and they typically progress to form discrete areas of RPE atrophy over their natural life cycle (9). Regions affected by flecks show reduced functionality (67). Another significant FAF feature is the identification of regions with decreased autofluorescence (DAF). These regions display varying levels of darkness in comparison to the absence of FAF signal seen in blood vessels and the optic nerve head. To classify these lesions, two categories are used: definitely decreased autofluorescence (DDAF) and questionably decreased autofluorescence (QDAF). In the grayscale, the optic nerve head (or, if not present in the image, blood vessels) serves as the reference point for 100% blackness. For a lesion to be classified as DDAF, it must appear more than 90% black when referenced to the optic nerve head. Conversely, QDAF lesions exhibit 50% to 90% blackness in comparison to the optic nerve head (68). The transition of QDAF lesions into DDAF may suggest the clearance of residual acellular lipofuscin material located subretinal. The measurement of DDAF area has been used as an endpoint in natural history studies to investigate predictors of atrophy expansion rate (10,69,70) (Figure 9).

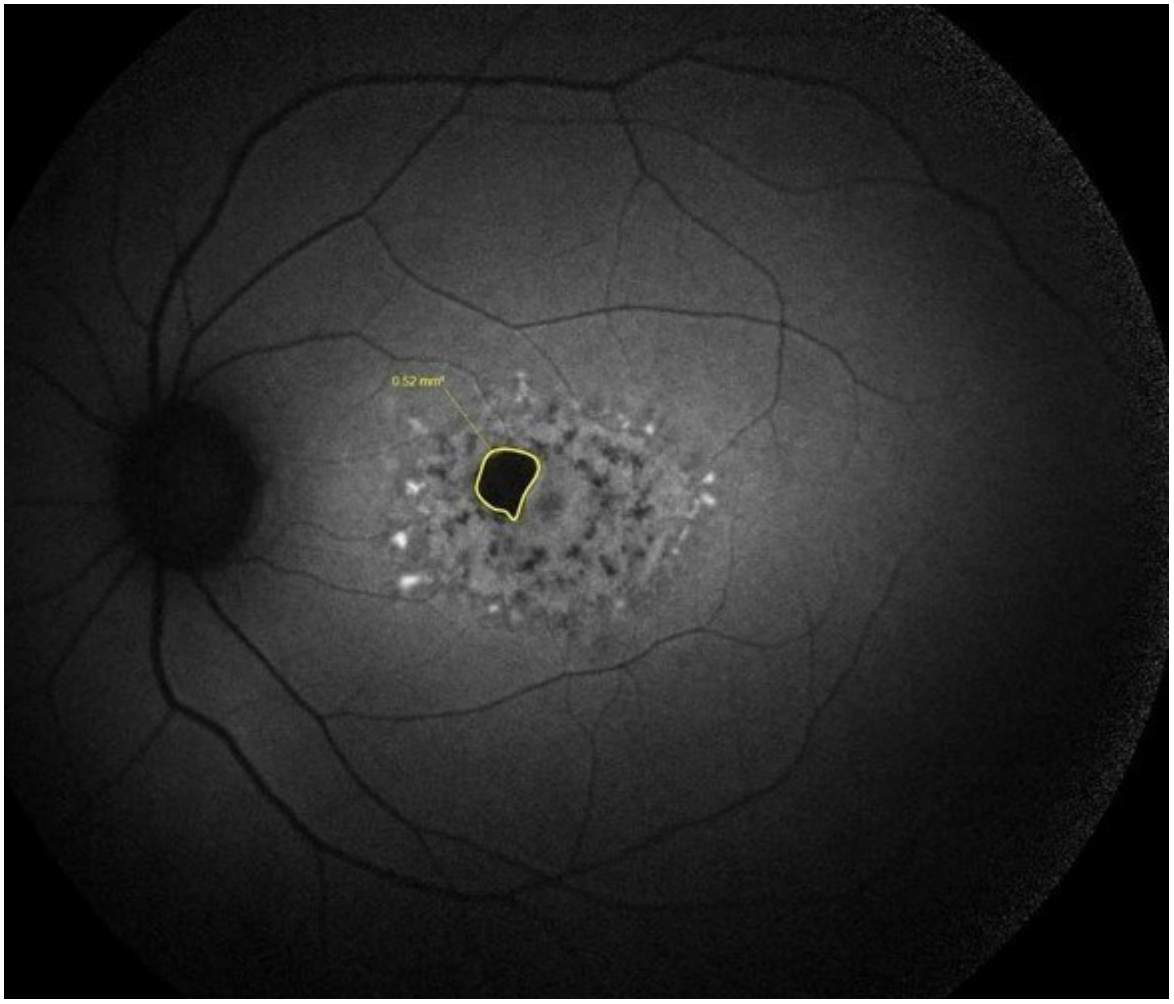

Figure 9: Fundus autofluorescence image of the posterior pole of a left eye with Stargardt's disease type 1, showing definitely decreased autofluorescence (DDAF) of 0.52mm^2 as highlighted with a yellow circle, an area of hyperautofluorescent and hypoautofluorescent dots centrally.

1.8.4 Electroretinography

Electrophysiological assessment plays a crucial role in offering more informed prognostic insights into STGD.

However, a limitation of this broad approach is its inability to detect subtle changes in the macula, which significantly contribute to the overall electrophysiological response of the retina. The multifocal electroretinogram (mfERG) provides greater precision as it allows for the simultaneous recording of local ERG responses from numerous well-defined retinal regions (9).

A classification based on electroretinography findings has been well-established, which categorizes patients into three functional phenotypes:

- Group 1: Characterized by severe pattern electroretinography abnormalities indicative of macular dysfunction, with normal full-field electroretinography (ffERG).
- Group 2: Displaying severe pattern electroretinography abnormalities along with additional generalized cone dysfunction observed in ffERG.
- Group 3: Exhibiting severe pattern electroretinography abnormalities in addition to generalized cone and rod dysfunction evident in ffERG.

Patients belonging to group 1 generally exhibit better visual acuity and a more limited distribution of flecks and atrophy. Conversely, those in group 3 tend to have the poorest visual acuity and a broader presence of flecks. Notably, macular atrophy is universally observed in group 3. However, there is a significant degree of overlap in these characteristics across the different groups (71).

1.8.5 Adaptive Optics Scanning Light Ophthalmoscopy

Recently, adaptive optics scanning light ophthalmoscopy (AOSLO) has emerged as a valuable research imaging technique that enables cellular-level visualization of the retina. AOSLO imaging can be categorized into two types: confocal and split-detector. Confocal imaging relies on the presence of an intact photoreceptor outer segment, where dark areas indicate cellular loss as opposed to outer segment loss. In contrast, SD-AOSLO only necessitates the presence of intact inner segments (72). In the context of Stargardt macular dystrophy (STGD), dark areas observed on confocal AOSLO imaging may reveal intact inner segments when examined using SD-AOSLO. However, it's worth noting that on split-detector imaging, these inner segments may appear "swollen" (73). Consequently, the condition of both the outer and inner segments may hold significance when considering the timing and eligibility of therapeutic interventions.

1.9 Therapy

At present, there remains a lack of established treatments to effectively stop or reverse maculopathy associated with Stargardt's disease. It is crucial to diagnose the condition early to facilitate low vision interventions, implement vocational and educational adjustments, and consider family planning. In certain instances, the specific genotype of the patient may hold prognostic value.

1.9.1 Gene Therapy for Stargardt Disease

With numerous ongoing clinical trials and the approval of gene therapy for inherited retinal diseases, the accumulation of evidence supporting the safety and efficacy of such an approach continues to grow each year. The primary focus so far has been on gene supplementation strategies for genes responsible for autosomal recessive diseases, like *RPE65* (74) , and X-linked disorders such as *CHM* (75) and *RPGR* (76), which are well-suited to this approach. While STGD1 appears to be a promising candidate for gene supplementation, the challenge lies in its large 6.8 kb coding sequence of *ABCA4*. Gene delivery is typically accomplished using adeno-associated virus (AAV), which has an optimal packaging capacity of around 4.7 kb (77). This limitation has prompted the development of various strategies to facilitate the delivery of larger genes. In contrast, both *ELOVL4* and *PROM1* coding sequences are of a size that can be efficiently packaged into AAV, but as they are primarily associated with autosomal dominant diseases featuring dominant negative mechanisms (33), gene supplementation is unlikely to resolve the disease condition. In the absence of generic pharmaceutical interventions, it is probable that treatment options for STGD3 and STGD4 will depend on future gene-editing technologies.(13).

1.9.2 Pharmaceutical Interventions

Small molecule therapies offer the possibility to target specific stages in the visual cycle or aspects of retinal function that are affected by Stargardt disease. While these therapies may not provide a cure, their objective is to alleviate symptoms and slow down the progression of the disease. Due to the intricate nature of the visual cycle and the distinct functions of *ABCA4*, *ELOVL4*, and *PROM1*, identifying suitable generic candidates has presented challenges. Nonetheless, there are currently several clinical trials exploring compound therapies that intervene in crucial pathological pathways associated with Stargardt disease.(13).

1.9.3 CRISPR

Researchers have adopted various strategies to address vision loss in individuals affected by Stargardt disease. While many potential treatment options have shown promise, it is possible that the most effective therapy has yet to be developed. Recent discussions have focused on the potential of clustered regularly interspaced short palindrome repeat (CRISPR)-based molecular tools, particularly their application in treating inherited retinal diseases (78–80). The ongoing discovery of new Cas proteins from different bacterial sources and the development of fusion

proteins to expand the molecular capabilities of these proteins mark the beginning of a new era in gene therapy. In the context of Stargardt disease, a significant portion of mutations in *ABCA4*, *ELOVL4*, and *PROM1* could potentially be targeted using one or more of the CRISPR-based approaches (13).

Despite the substantial number of Stargardt disease patients, particularly those with STGD1, the development of an effective treatment has lagged behind that of other, rarer recessive inherited diseases. While numerous encouraging therapies have been evaluated in trials thus far, it is conceivable that the most efficacious treatment may be realized through CRISPR-based approaches. Regardless of the chosen approach, the collective efforts undertaken thus far provide optimism that an effective treatment for Stargardt disease may emerge in the coming years (13).

While an approved therapy for STGD4 is currently unavailable (81), there is a pressing need for robust outcome measures, such as monitoring disease progression or tracking changes in retinal layers over time, to support future therapeutic endeavours. To identify potential endpoints and to enhance our comprehension of the natural course of STGD4, the "Natural History of the Progression of Atrophy Secondary to Stargardt Disease type 4 (STGD4): A Prospective Longitudinal Observational Study of Stargardt Disease type 4, PROM1-related Dystrophy" (ProgStar-4 Study) was initiated (82).

Visual acuity represents the most commonly employed clinical endpoint in ophthalmic research (12); However, it possesses several limitations when applied to inherited retinal dystrophies. These limitations encompass slow or delayed disease progression, the presence of stable plateau phases, and a substantial reliance on stable fixation and the precise location of atrophic alterations (12). An analysis of the progression of *ABCA4*-related Stargardt disease (ProgStar) cohort has revealed that visual acuity is not a suitable primary outcome measure for clinical trials. Instead, it should be considered only for specific subgroups (4). Consequently, surrogate endpoints derived from retinal imaging techniques have become imperative and have garnered endorsement from regulatory authorities, particularly for the treatment of macular diseases (83). SD-OCT imaging offers the ability to visualize distinct retinal and choroidal layers, facilitating the detection of morphological intraretinal alterations that manifest in macular diseases. As a

result, SD-OCT changes have been designated as secondary endpoints in the ProgStar-4 study (82). In this context, we present the estimated rates of atrophy progression derived from the analysis of SD-OCT images.

2 Methods

Our cohort was comprised of a carefully selected group of individuals, a total of 15 right eyes of 15 patients, who met specific criteria for inclusion. These criteria included an age of 6 years or older at the study's baseline, as well as confirmed genetic variants in the *PROM1* gene, directly linked to retinal changes associated with STGD4.

These fifteen right eyes, serving as our focal point for analysis, presented a unique opportunity to gain insights into the natural progression of this rare and complex genetic disorder. Their initial assessments marked the commencement of our investigation, setting the stage for a comprehensive evaluation of retinal health and atrophic changes over time.

Over the course of 24 months, our study diligently monitored the evolution of retinal atrophy and change in individual retinal layer thickness in these patients. This involved the utilization of SD-OCT, an imaging technology that offers high-resolution and non-invasive cross-sectional views of the retina. By meticulously analysing the SD-OCT images we aimed to unravel the dynamic changes in mean thickness and intact area occurring within individual retinal layers.

2.1 Ethics

The study was conducted according to the International Conference on Harmonisation of Technical Requirements for Registration of Pharmaceuticals for Human Use good clinical practice (GCP) Guidelines, the applicable regulatory requirements, and the current Declaration of Helsinki (84) and was in compliance with the Health Insurance Portability and Accountability Act if applicable. Ethics committee approval was granted by the local institutional review boards of the participating sites and received approval from the Ethics Committee of the Medical University of Graz (EC number: 31-081 ex 18/19).

All patients gave informed consent before enrolment.

2.2 Clinical Centers

Patients were recruited at 5 centers in the USA, UK, and Germany. A custom-built database in REDCap (http://www.projectredcap. org/cite.php) served at a central database in which all data were entered and checked for completeness and consistency by the data coordinating center. Investigators at each clinical center identified potential study patients from their own patient populations, referral from other ophthalmologists or by self-referral. Participation was open to all interested patients and made public using an openly accessible internet webpage (http://progstar.org/progstar-home/progstar-4/).

2.3 Quality Assurance and Methods to Minimize Bias

The eligibility of patients was verified by the principal investigator at each study site. Data collection and procedures were standardized and detailed in the study manual of procedures. Prior to the study's commencement, all personnel involved in conducting study procedures underwent training and certification. The quality and completeness of the acquired images were evaluated by the Reading center (RC), and if any issues such as poor quality or missing images were identified, the photographers at the participating centers were notified. Image graders were not blinded to the sequence of visits or patient identity. Two graders, both certified by the RC, independently reviewed the images, and in cases of disagreement, an adjudication process was employed, with the final decision made by an RC investigator. Subsequently, all data generated from grading were transferred from the RC to the data coordinating center using the REDCap system. Case report forms were maintained at each study site.

2.4 Inclusion Criteria

In the pursuit of scientific inquiry and the advancement of medical knowledge, the formulation of rigorous and well-structured inclusion criteria is of paramount importance. In this study, we have carefully delineated a set of specific criteria that define the population under investigation, ensuring the precision and validity of our research outcomes. These criteria served as a gateway, allowing us to focus on patients and participants who best align with the objectives of the study.

- Patients with suspected or confirmed STGD4, carrying mutations in the *PROM-1* gene (preferably with dominant inheritance) were eligible for inclusion in this study.
- Participants were required to provide a signed informed consent form and authorization permitting the disclosure and use of protected health information.
- The primary study eye needed to exhibit at least one well-demarcated area of atrophy, with the lesion size not exceeding the area to be tracked in the SD-OCT mode (20x20 degrees).
- Confirmation of at least one pathogenic mutation in the *PROM1* gene, along with a diagnosis of Stargardt phenotype, was essential.
- The primary study eye had to have clear ocular media and adequate pupillary dilation, as determined by the investigator, to enable high-quality SD-OCT imaging.
- Participants were required to be capable of cooperating during the examination procedures.
- Willingness to undergo ocular examinations for a duration of 24 months was necessary.
- Participants needed to be at least six years old, and both eyes could be included if they met the inclusion criteria. There were no restrictions on visual acuity for eligibility in the study.

These inclusion criteria collectively define the parameters within which our study was conducted, emphasizing the precision and integrity of our research methodology. By adhering to these criteria, we aimed to generate findings that are robust, reliable, and ultimately contribute to the advancement of our understanding of STGD4 and its genetic underpinnings.

2.5 Exclusion Criteria

In this study, a careful and considered selection of exclusion criteria has been established to ensure the accuracy, reliability, and ethical conduct of our research. These exclusion criteria serve as gatekeepers, preventing the inclusion of individuals who may introduce confounding factors or ethical concerns.

- Presence of ocular diseases, such as choroidal neovascularization, glaucoma, and diabetic retinopathy, in either eye that may interfere with the accurate assessment of retinal morphology and function.
- Patients who underwent intraocular surgery in the primary study eye within 90 days preceding the baseline visit.
- Current or prior participation in an interventional study for the treatment of STGD, such as gene therapy or stem cell therapy. Current involvement in a drug trial or participation in a drug trial within six months prior to enrolment. The use of oral vitamin and mineral supplements was allowed, but the current use of Vitamin A supplementation had to be documented.
- The site Principal Investigator was able to deem any patient at their site ineligible for study participation based on valid medical reasons before the patient's enrolment.
- Presence of any systemic disease with a limited prognosis for survival (e.g., cancer, severe/unstable cardiovascular disease).
- Any condition that would have hindered the patient's ability to adhere to the examination schedule, making it difficult or unlikely for them to attend regular follow-up visits for up to 24 months. Examples include personality disorders, use of major tranquilizers like Haldol or Phenothiazine, chronic alcoholism, Alzheimer's Disease, or drug abuse.
- Evidence of significant uncontrolled concurrent diseases such as cardiovascular, neurological, pulmonary, renal, hepatic, endocrine, or gastrointestinal disorders.

In summary, these exclusion criteria are meticulously defined to maintain the scientific rigor, ethical standards, and safety of our study. By adhering to these criteria, we strive to ensure the reliability and validity of our research, ultimately contributing to the advancement of knowledge in the field of ocular and systemic health.

2.6 Sample Size

The modest sample size in this study can be primarily attributed to the rare prevalence of STGD4. This particular genetic disorder is known for its exceptional rarity, affecting only a very limited number of individuals worldwide. In fact, the global literature has recorded a mere 41 documented cases of STGD4 at time of launching the study, underscoring the challenges associated with assembling a sizable study population for this specific condition (31)

Given the scarcity of STGD4 cases, recruiting a sufficiently large sample is inherently challenging. Nevertheless, the research team diligently sought individuals who both expressed a willingness to participate and met the rigorous pre-established criteria for inclusion and exclusion. The inclusion criteria were thoughtfully designed to identify those individuals who could provide valuable insights into the condition and contribute to the study's objectives while ensuring the scientific integrity and validity of the research findings. Conversely, the exclusion criteria were established to exclude individuals who might introduce confounding factors or pose ethical concerns.

The combination of the condition's rarity and the strict eligibility criteria underscores the considerable effort and precision involved in recruiting participants for this study. Despite the challenges posed by the limited number of documented cases, the commitment to advancing our understanding of STGD4 remains unwavering, and every eligible participant's contribution is invaluable in shedding light on this uncommon and complex genetic disorder.

2.7 Objective

This study has a primary objective aimed at providing a comprehensive and longitudinal investigation into the alterations in individual retinal layer thickness and the preservation of the intact retinal area in patients suffering from STGD4. We have chosen to employ the advanced technology of SD-OCT as our primary tool for meticulously tracking these retinal changes over a prolonged 24-months period.

Retinal layer thickness serves as a vital indicator of the health and integrity of the retinal structure. Understanding how these thicknesses change over time is crucial in diagnosing and managing various retinal conditions. Additionally, the extent of the intact retinal area is equally pivotal as it reflects the preservation of functional, non-damaged retinal tissue. This is

especially relevant in conditions like Stargardt disease, where the preservation of such areas is critical for maintaining vision.

By utilizing SD-OCT, a highly precise imaging modality, we aimed to capture the most nuanced changes in retinal layer thickness and the extent of the intact retinal area. This technology employs non-invasive, high-resolution imaging to provide detailed cross-sectional views of the retina, allowing for the quantification of these vital parameters.

The 24-month duration of our study is crucial, as it offers an extended and comprehensive insight into the temporal evolution of these retinal alterations. This extended time frame enables us to detect subtle changes and understand the progression of these changes, which can be invaluable in the context of retinal diseases. Furthermore, such long-term data can provide insights into the efficacy of potential treatments, making it an essential aspect of our study design.

In essence, this study has set out to explore the dynamic nature of retinal layer thickness and the preservation of the intact retinal area over a 24-month period. Through the application of state-of-the-art SD-OCT technology, we aspire to gain a deeper understanding of how these parameters change over time, with the ultimate goal of enhancing our knowledge of retinal health and contributing to the advancement of eye care and disease management.

2.8 SD-OCT and Grading Modalities

In our investigation, a multi-center approach was employed to obtain a rich dataset of retinal scans using the advanced Heidelberg SpectralisTM device. At the outset of our study, during the baseline assessment, this state-of-the-art technology was utilized to capture detailed images covering a specific scan area measuring 20° x 20°. This area was meticulously composed of 49 B-scans, with the anatomical fovea serving as the central point of reference.

Our investigation extended over a period of 24 months, after which a follow-up scan was conducted using the built-in follow-up mode of the Heidelberg SpectralisTM device. This longitudinal approach enabled us to track changes and progressions in retinal layers analysed.

Throughout our data collection process, we upheld rigorous standards for image quality, excluding any scans that did not meet the predefined criteria, commonly referred to as "ungradable images." The focus on image quality was fundamental to ensure the reliability and accuracy of our subsequent analyses.

The heart of our study lay in the meticulous analysis of SD-OCT scans, with a particular emphasis on changes in the mean thickness and intact areas of specific retinal layers. These parameters held the key to understanding the progression of retinal atrophy and were assessed at two critical time points: baseline and after 24 months.

To provide a structured framework for our analysis, we adopted the well-established "Early Treatment Diabetic Retinopathy Study" (ETDRS) grid, defining three specific regions of interest: the central subfield (CS) with a 0.5mm radius, the inner ring (IR) spanning 0.5 to 1.5mm, and the outer ring (OR) extending from 1.5 to 3mm from the fovea. These delineated regions allowed us to focus our investigations with precision.

It's important to note that, to maintain consistency and relevance in our analysis, we exclusively included results from retinal locations that could be imaged at both baseline and the 24-month follow-up. In cases where patients experienced a shift in their preferred retinal locus during the observation period, resulting in the imaging of a different retinal region, especially within the outer ring area, those regions were thoughtfully excluded from our analysis.

Moreover, we opted to direct our efforts toward the right eyes of our participants, designating them as the main focus of our study. This strategy enabled us to maintain a uniform and concentrated analysis of particular retinal changes and atrophic patterns, particularly considering that *PROM1*-associated retinopathy typically affects both eyes symmetrically. We assessed all 15 patients in our cohort for symmetry between their right and left eyes, which was evident in every patient.

In summary, our multi-center study represents a comprehensive and methodical exploration of retinal health, leveraging advanced imaging technology to capture the dynamic progression of specific retinal layers over a 24-month period. Our rigorous standards for data quality, detailed analysis of distinct regions, and the exclusive focus on right eyes as primary study eyes collectively form the foundation of our study, aimed at advancing our understanding of retinal conditions and facilitating enhanced clinical care and management.

2.8.1 Boundaries

To ensure the quality of our data, we required a minimum of 25 B-scans per cube scan, per eye, and per visit. The selection of scans for inclusion was determined by the grader, taking into account their similarity to adjacent B-scans. If adjacent B-scans exhibited noticeable qualitative differences in retinal sublayer thicknesses, both were included. However, if they closely resembled each other, a gap of more than one B-scan between selected B-scans was allowed. Nevertheless, it was mandatory to include all B-scans from the fovea center, which corresponds to the central subfield of the ETDRS-grid. (85). When dividing the subsequent retinal layers from anterior to posterior, the term "inner" corresponds to the inner boundary and "Outer" to the outer boundary of a layer (Figure 10):

- Vitreous Top (VT) – The Doheny Image Analysis Laboratory's classification algorithm inserts an additional boundary "Vitreous Top" in the vitreous space. This boundary (+ ILM) is used to quantify the area of the visible ETDRS grid when the grid is centered on the fovea. These area values can be used to detect poor foveal centration of the scan.
- Inner Limiting Membrane (ILM) – Inner
- Outer Plexiform Layer (OPL) – Outer
- External Limiting Membrane (ELM)
- Inner Segment-Outer Segment Junction (IS-OS) or ellipsoid zone (EZ) – Outer
- Photoreceptor Segment Layer (PRS) –The PRS boundary was manually modified on the inner side of any subretinal fluid or material at the level of the RPE. In cases without any fluid or debris this boundary was snapped with the RPE boundary.
- Retinal Pigment Epithelium (RPE) Cell Layer – Inner
- Choroid – Inner

Adapted from Grosspoetzl et al. with permission of Elsevier under the terms of the Creative Commons CC-BY license (1)

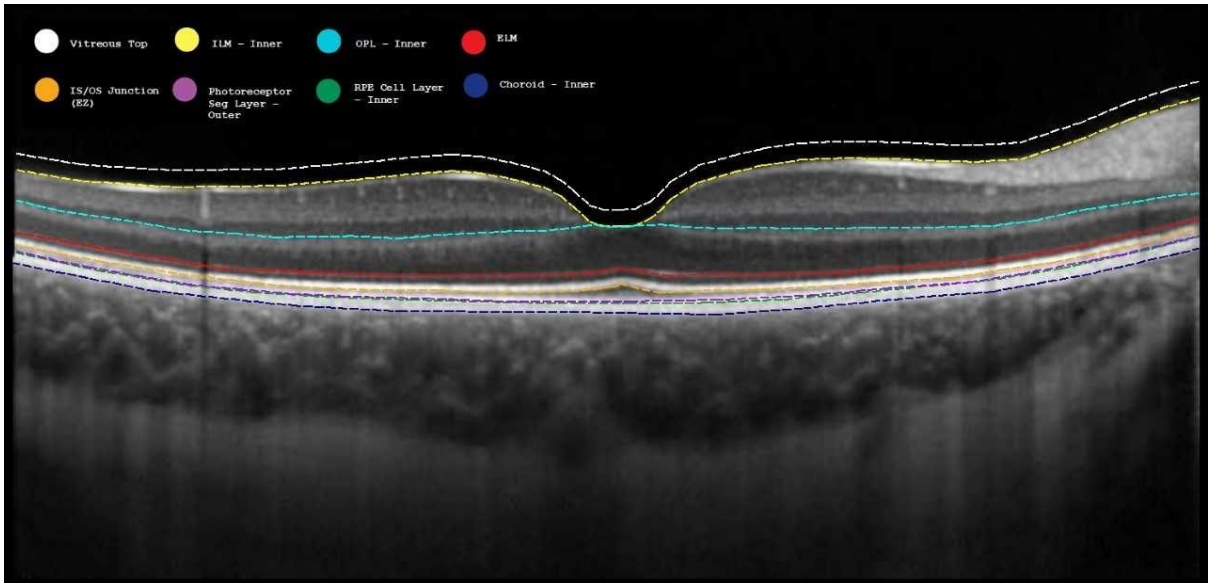

Figure 10: Example of a B-scan (spectral domain optical coherence tomography) of a healthy eye showing the segmented boundaries of retinal sublayers.

By employing these boundaries, we delineated and computed the following layers, their thicknesses, and intact areas (Figure 11):

- Mean inner retinal thickness (IR): generated from ILM and OPL
- Mean ONL thickness (ONL): generated from OPL and ELM.
- Mean IS thickness (IS): generated from ELM and IS-OS junction
- Mean OS thickness (OS): generated from IS-OS Junction and RPE cell layer
- Mean RPE thickness and intact area: generated from RPE and Choroid
- Mean total retinal thickness (TR) and intact area: generated from ILM and choroid

This correction process was a collaborative effort, involving the insights and expertise of two unmasked graders, denoted as MG and GS. These diligent individuals meticulously reviewed and, when necessary, adjusted the algorithm's segmentation results to align with the precise anatomical boundaries of the retinal layers.

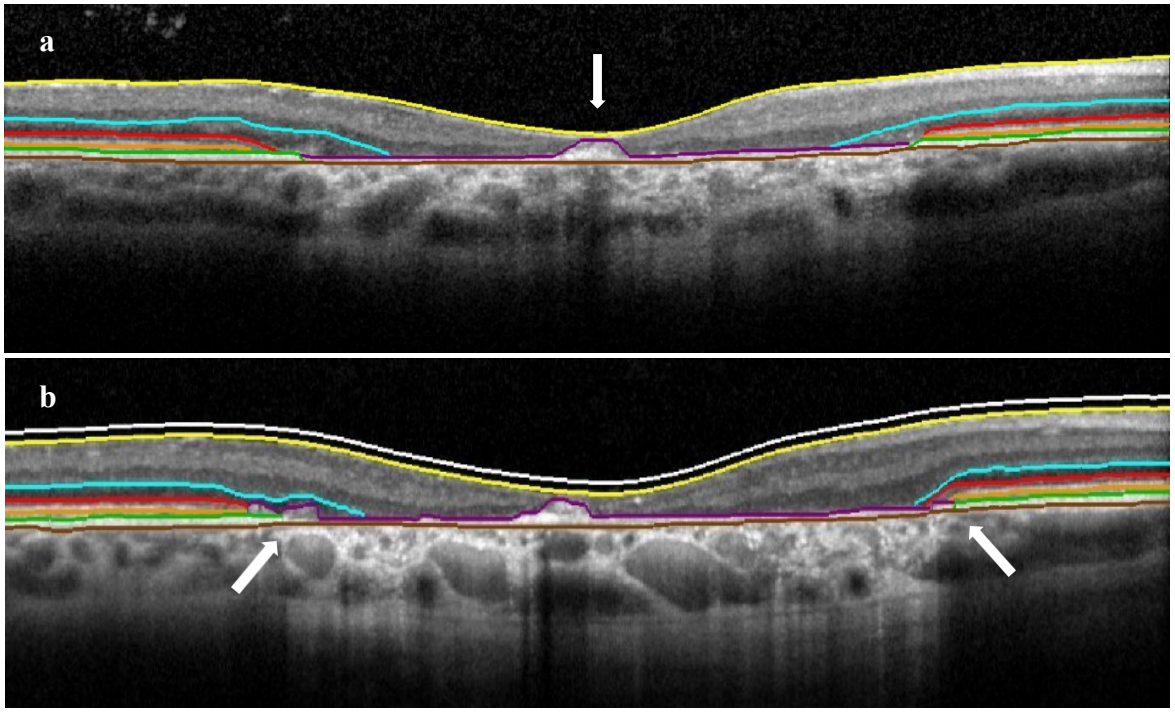

Figure 11: Segmentation of a patient's right eye diagnosed with Stargardt disease type 4 overlaid SD-OCT B-scans after manually segmentation at baseline and after 24 months. The segmented layers in order from top to bottom are: vitreous top=white; internal limiting membrane=yellow; outer plexiform layer=blue; external limiting membrane=red; inner segments/outer segments=orange; photoreceptor segment layer=purple; retinal pigment epithelium=green; choroid=brown. (**a**) SD-OCT B-scan of a patient's right eye showcasing an atrophic lesion of the outer retinal layers and central debris highlighted by the white arrow at baseline and (**b**) exhibits the SD-OCT B-scan of the same eye.

Adapted from Grosspoetzl et al. with permission of Elsevier under the terms of the Creative Commons CC-BY license (1)

2.9 OCTOR

In our study the Doheny Image Analysis Laboratory's (DIAL) classification algorithm was applied. This advanced, automated segmentation algorithm was purposefully crafted to dissect the intricate layers of the retina, utilizing high-resolution SD-OCT scans. The algorithm's primary function was to delineate and define individual retinal layers.

However, recognizing the critical importance of error correction and the nuances that may elude automated systems, we implemented a meticulous protocol to address any segmentation discrepancies that might arise. To this end, we engaged in manual correction processes, leveraging the specialized software tool OCTOR 3.0.

In instances where discrepancies or uncertainties emerged during this manual correction phase, the matter was elevated for resolution. A senior investigator of the study, referred to as RWS,

served as the ultimate authority in addressing any disagreements or complex cases. This consultative process ensured that the segmentation outcomes were not only accurate but also reflective of a consensus among experienced professionals.

Following the meticulous correction of segmentation errors, the refined software was primed to fulfil its primary functions. This included the computation of thickness measurements for various retinal layers, a critical component of our investigation. Additionally, the software was adept at identifying and delineating areas of atrophy within the retinal layers, aligning with the regions specified in our study's methodology (Figure 12 and Figure 13).

In essence, our approach combined the strengths of advanced automated algorithms with the vigilance and expertise of human graders to ensure the integrity and accuracy of our data. This robust methodology allowed us to extract meaningful insights into retinal health and atrophy, ultimately contributing to the broader understanding of retinal diseases and the enhancement of diagnostic and therapeutic strategies in STGD4.

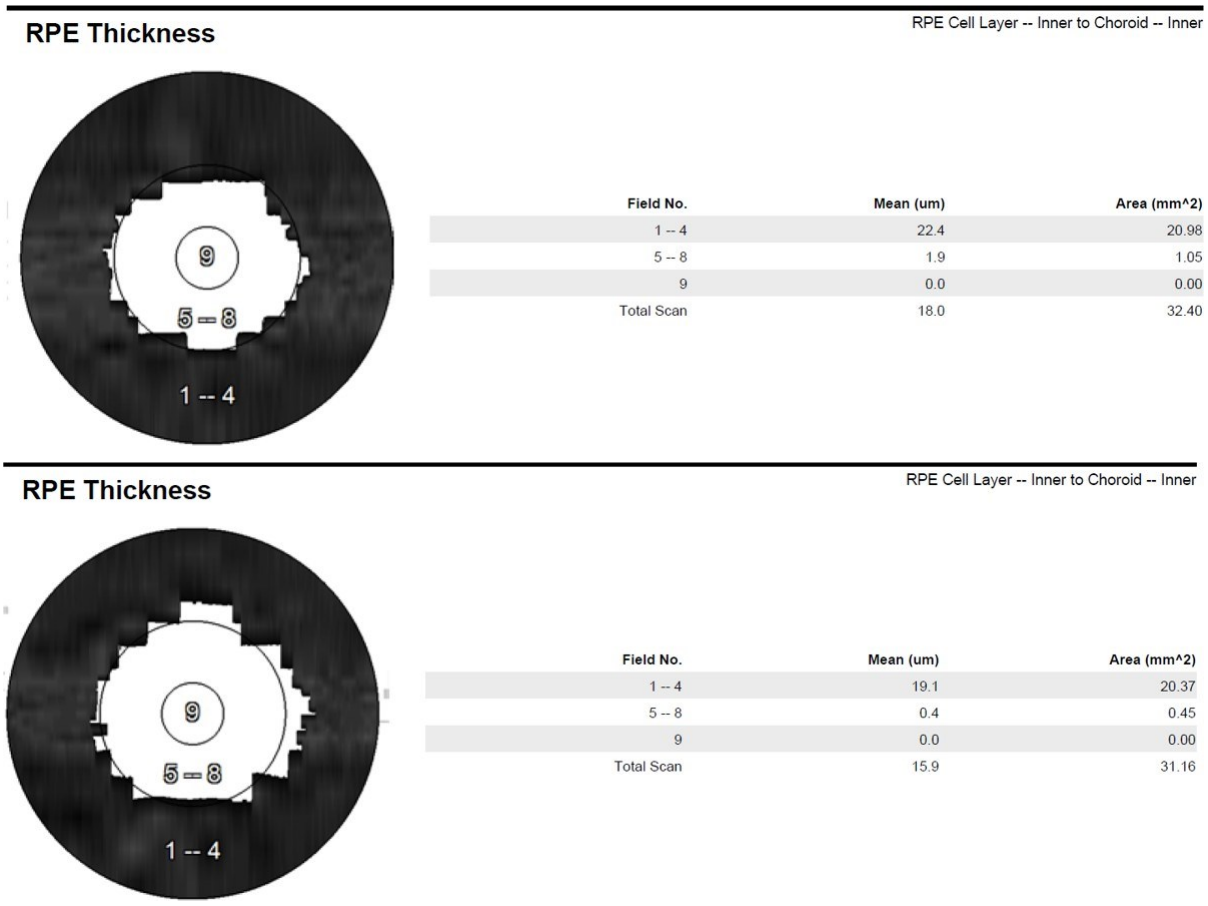

Figure 12: The OCTOR report presents the assessment of a patient's right eye initially and after 24 months, following the automated segmentation of spectral domain optical coherence tomography (SD-OCT) images utilizing the Doheny Image Analysis Laboratory's classification algorithm for segmentation. Subsequently, manual adjustments were made to the retinal pigment epithelium (RPE) area defined between the RPE inner segment and the Choroid inner segment. Notably, a reduction in the intact area, characterized by an increase in the white area in the central subfield, both the inner and outer rings of the early treatment diabetic retinopathy study (ETDRS) grid, was observed. Additionally, a decrease in the mean retinal thickness of the RPE became apparent. At the baseline visit, the mean thickness of the RPE in the central subfield had already completely diminished, registering 0.4 µm in the inner ring and 19.1 µm in the outer ring. The intact area of the RPE was entirely atrophied in the central subfield, measuring 0 mm^2, while the inner ring had an intact RPE area of 0.45 mm^2, and the outer ring showed an intact RPE area of 20.37 mm^2. This demonstrated a reduction of 1.5 µm in mean RPE thickness in the inner ring and 3.3 µm in the outer ring over the observed 24 months period. The intact area in the inner ring exhibited a decline of 0.6 mm^2, and in the outer ring, it showed a decrease of 0.61 mm^2 over the 24 months period. Notably, in the central subfield, no changes were observed in the mean thickness of the RPE and the intact RPE area, as it had already fully atrophied before the baseline visit.

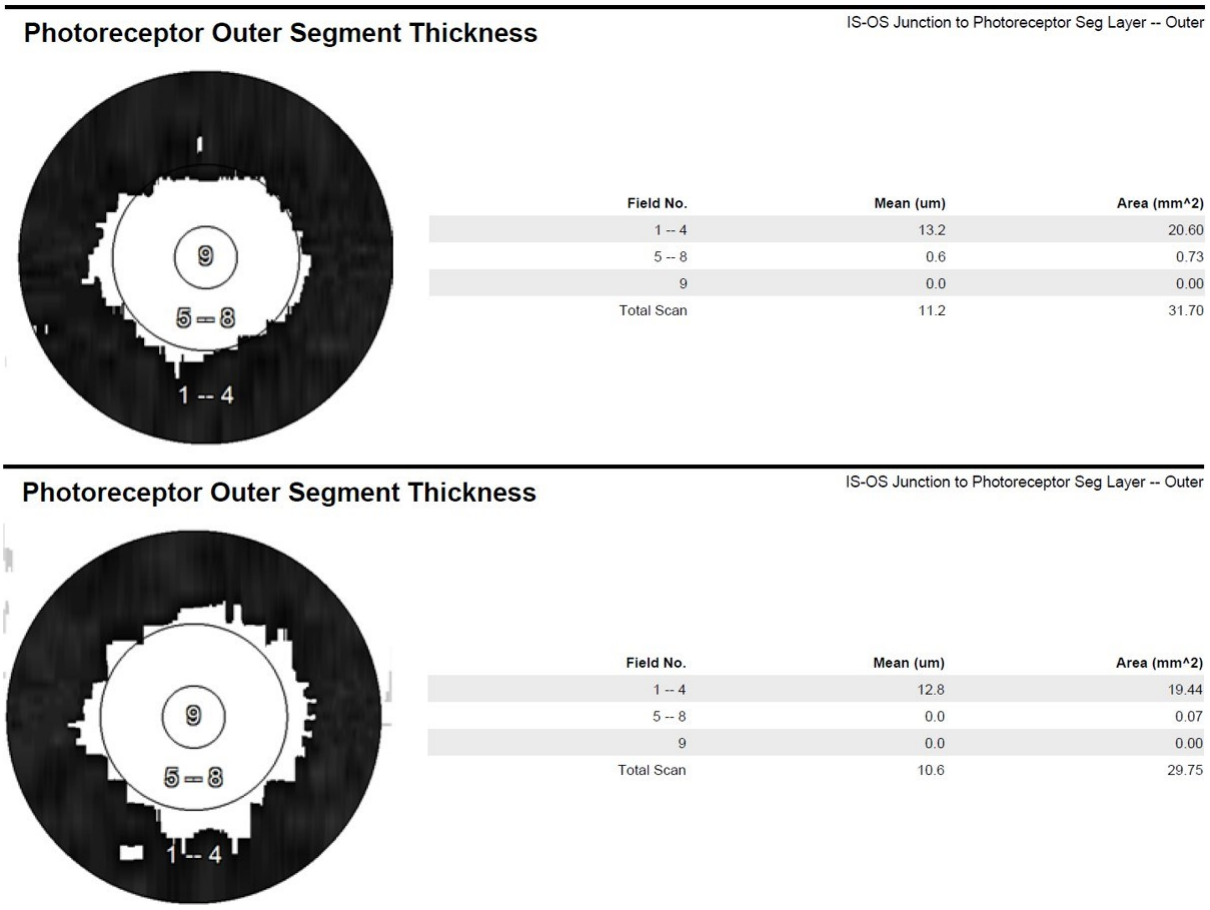

Figure 13: The OCTOR report details the evaluation of the same eye as depicted in Figure 13, both initially and after a 24-month interval, following the automated segmentation of spectral domain optical coherence tomography (SD-OCT) images utilizing the classification algorithm by the Doheny Image Analysis Laboratory. Subsequent manual adjustments were applied to the photoreceptor outer segment thickness (OS) area, which was generated from the inner segment-outer segment (IS-OS) Junction outer side, as well as the retinal pigment epithelium (RPE) cell layer inner segment. Remarkably, a decrease in the intact area, marked by an expansion of the white area within the inner and outer ring of the early treatment diabetic retinopathy study (ETDRS) grid, was evident over the 24-month period. Furthermore, a reduction in the mean retinal thickness of the OS became noticeable. During the baseline visit, the mean thickness of the OS in the central subfield had already fully diminished, measuring 0.6 µm in the inner ring and 13.2 µm in the outer ring. The intact area of the OS had completely atrophied in the central subfield, resulting in a measurement of 0 mm^2. In contrast, the inner ring displayed an intact OS area of 0.73 mm2, while the outer ring featured an intact OS area measuring 20.60 mm^2. After 24 months, a reduction of 0.6 µm in mean OS thickness within the inner ring and 0.4 µm within the outer ring became evident. The intact area within the inner ring demonstrated a decline of 0.66 mm^2, whereas the outer ring exhibited a decrease of 1.16 mm^2 over the 24 months period. Notably, in the central subfield, there were no observable changes in the mean thickness of the OS and the intact OS area, as it had already fully atrophied prior to the baseline visit.

2.10 Qualitative Grading Considerations

In retinal imaging, a detailed understanding of various structural features and anomalies is paramount to unravelling ocular health. Within this context, our exploration delves into a spectrum of distinctive attributes that manifest within the retinal layers and the vitreoretinal interface. These features, when observed in SD-OCT images complicate the segmentation and were specially taken in consideration in our study.

2.10.1 Intraretinal Cystoid Spaces

Intraretinal cystoid spaces are commonly colloquially termed retinal cysts. They represent distinct regions of reduced reflectivity within the neurosensory retina. Typically, these spaces exhibit a circular or oval morphology.

2.10.2 Subretinal Fluid

Subretinal fluid (SRF) appears as reflective posterior to the neurosensory retina, but anterior to the RPE. Oftentimes, hyporeflectivity of the space is comparable to that of the vitreous; however, the space may not be completely hyporeflective, e.g. it may contain blood cells or fibrinous tissue. There are often tapered corners at the margins of this hyporeflective space, although in the setting of inflammatory diseases or extensive fibrinous exudation, the margins may feature a more acute angle.

2.10.3 Intraretinal Hyperreflective Features

Intraretinal hyperreflective features, characterized by small clusters of hyperreflective material within different layers of the retina, may indicate the presence of intraretinal lipid, pigment, foreign bodies, or hemorrhage. These dense features typically result in pronounced posterior shadowing, especially in the case of lipid and, to a lesser extent, hemorrhage.

2.10.4 Epiretinal Membrane

Epiretinal membrane (ERM) manifests as a slender, hyperreflective band located at the vitreoretinal interface, frequently displaying points of attachment and detachment from the inner limiting membrane. ERM commonly exerts tension or causes a wrinkling effect on the inner retinal surface, resulting in an irregular or "bumpy" appearance, hence its occasional colloquial reference as "macular pucker."

2.10.5 Vitreomacular Traction

Vitreomacular traction is characterized by the presence of a slender, hyperreflective band extending from the posterior hyaloid of the vitreous, seemingly inserting into the retina and exerting traction. To classify as vitreomacular traction, it is essential that the vitreous is the predominant factor causing the deformation of the retinal contour, typically marked by a peak at the attachment point.

2.10.6 Outer Retinal Tubulation

Photoreceptors that have sustained damage, possibly due to the disruption of their interdigitation with the RPE or RPE degeneration itself, can assume a circular or oval arrangement. This phenomenon, referred to as outer retinal tubulation (ORT), manifests as a hyporeflective (sometimes hyperreflective) oval structure enclosed by a hyperreflective circular border. It's important to note that outer retinal tubules may be mistaken for edema; however, a key distinguishing characteristic is the presence of the hyperreflective rim. This specific morphological feature is rarely observed over intact RPE but is more commonly seen over RPE that has undergone atrophy.

2.10.7 RPE Atrophy

Detecting RPE atrophy and its boundaries in OCT images can be challenging. When RPE atrophy is present, some common features include:

- Increased signal transmission into the choroid: Due to the absence of the highly reflective RPE layer, more light can penetrate into the choroid and bounce back.
- Collapse or absence of outer retinal layers, such as the EZ and ELM.
- Abnormal thinning of the retina.
- Thinning of the RPE compared to adjacent, undisturbed RPE.
- Presence of outer retinal tubules overlying the atrophic area.
- Presence of small, hyporeflective cystoid spaces overlying the affected region.

2.11 Statistical Methods

Categorical data is presented with quantity and percentage and continuous data with mean and standard deviation. To evaluate the change over time (baseline - 24 months) linear models for repeated measures with endpoints (mean retinal thickness and intact area values) on original

scale and square root transformed endpoints (intact area values) as dependent variables and time as continuous independent variable were used. The beta coefficients for time represent the yearly progression rates and are displayed with their corresponding standard errors (SE). P- values < 0.05 were interpreted as statistically significant. SAS version 9.4 (SAS, Cary, North Carolina, USA) was used for statistical analysis.

3 Results

Images with insufficient quality (ungradable images) were excluded. In these patients, also the images of the left eyes showed insufficient quality for potential grading; hence, these patients were excluded. A total of 15 patients were enrolled into the study. Gradable images were available for 13 right eyes of 13 patients for both the baseline and the 24 months visit; information about disease-causing variants is provided in Table *1*. Out of these, six were males and seven females; mean age (± standard deviation, SD) at baseline was 38.2±14.2 years and mean age of onset of symptoms (available for twelve patients) was 30.3±16.3 years. Mean best-corrected visual acuity (±SD) at baseline was 0.51±0.53 LogMAR. Notably, our imaging methodology enabled us to consistently capture the same regions within the central subfield and inner ring for all eyes included in the study, ensuring the consistency and reliability of our data. In summary, our study is underpinned by a meticulously selected cohort of patients, characterized by their diverse demographics and precise imaging techniques. By focusing on the right eyes of these individuals and employing rigorous inclusion criteria, we aim to enhance our understanding of retinal health and contribute to the advancement of ophthalmological knowledge in STGD4.

3.1 Outcome Measures

In the pursuit of scientific understanding and meticulous assessment, this section of our study delves into a detailed analysis of various key parameters related to retinal thickness and integrity over a 24-months period using SD-OCT. These parameters encompass a comprehensive evaluation of the mean thickness and intact area of analysed retinal layers at baseline, the estimated yearly rate differences and has a particular focus on their progression patterns and statistical significance.

Table 1: Presented are the disease-causing variants in PROM1 in patients included in analysis of this study.

Adapted from Grosspoetzl et al. with permission of Elsevier under the terms of the Creative Commons CC-BY license (1)

Patient ID	Disease-causing variant 1	Disease-causing variant 2 (if applicable)
1	c.1117C>T	
2	c.1117C>T	
3	c.1117C>T	
4	c.1117C>T	
5	c.1354_1355 ins T	c.630_c.630+8 del 9 ins 13
6	c.1117C>T	
7	c.1117C>T	
8	c.1117C>T	
9	c.1697delA	c.1767+4A>G
10	c.963>T; p.Leu321Phe	
11	c.1117C>T	
12	c.1117C>T	
13	c.1117C>T	

3.2 Central Subfield of the ETDRS grid

The Central Subfield, a pivotal component of the ETDRS grid, is a meticulously defined region that holds significant clinical and research importance in the field of ophthalmology. This central portion, typically characterized by a 0.5mm radius around the anatomical fovea, serves as a focal point for the assessment and evaluation of retinal health and integrity.

Within the central subfield, the intricate and delicate layers of the retina are subject to scrutiny, with particular attention to changes in thickness, the presence of atrophy, and the integrity of individual retinal layers. The precise measurements and observations within this region offer critical insights in STGD4.

3.2.1 Mean thickness baseline (µm)

At the baseline visit, one eye (7.7%) had a mean thickness of 0 for ONL, 7 eyes (53.8%) had mean thicknesses of 0 for IS, 9 eyes (69.2%) had mean thicknesses of 0 for OS and 4 eyes (30.8%) had mean thicknesses of 0 for RPE.

The mean thickness of the IR was 89.83 (SD±16.61) µm, of the ONL 51.14 (SD±30.53) µm, of the IS 10.35 (SD±16.74) µm, of the OS 2.3 (SD±4.19) µm, of the RPE 13.35 (SD±12.73) µm and of the TR 183.75 (SD±48.81) µm at the baseline visit (Table 2).

3.2.2 Mean thickness - estimated yearly rate difference in progression

The estimated yearly rate difference of the IR revealed a change of -1.981 (SD±1.309) µm, of the ONL -1.112 (SD±1.056) µm, of the IS -0.481 (SD±0.405) µm, of the OS 0.060 (SD±0.082) µm, of the RPE -1.935 (SD±0.846) µm and of the TR -3.112 (SD±0.965) µm.
The RPE and the TR mean thickness showed statistically significant decline over 24 months (all $p<0.05$) (Table 2).

Table 2: Estimated annual decline rates in the central subfield, the inner ring and the outer ring of the progression of mean thicknesses [µm per year] of the examined retinal layers.

Adapted from Grosspoetzl et al. with permission of Elsevier under the terms of the Creative Commons CC-BY license (1).

Retinal layers	**Baseline values of the mean thickness [µm], mean ± standard deviation**			**Estimated rate difference in progression [µm per year] of the mean thickness, coefficient ± standard error; p-value**					
	Central subfield	**Inner ring**	**Outer ring**	**Central subfield**	**p-value**	**Inner ring**	**p-value**	**Outer ring**	**p-value**
IR	89.83 ± 16.61	141.29 ± 21.02	132.96 ± 12.70	-1.981 ± 1.309	0.156	-0.542 ± 0.062	0.399	-0.029 ± 0.070	0.969
ONL	51.14 ± 30.53	42.44 ± 15.67	49.41 ± 16.62	-1.112 ± 1.056	0.313	-1.108 ± 0.651	0.114	-1.550 ± 0.481	**0.018**
IS	10.35 ± 16.74	7.18 ± 10.82	19.71 ± 15.19	-0.481 ± 0.405	0.259	-0.600 ± 0.288	0.059	-0.714 ± 0.238	**0.024**
OS	2.30 ± 4.19	1.38 ± 3.15	4.91 ± 4.63	0.069 ± 0.082	0.417	-0.135 ± 0.093	0.172	-0.307 ± 0.145	0.078
RPE	13.35 ± 12.73	14.35 ± 9.10	20.67 ± 4.60	-1.935 ± 0.846	**0.041**	-1.939 ± 0.511	**0.003**	-1.321 ± 0.917	0.200
TR	183.75 ± 48.81	222.11 ± 34.77	232.60 ± 34.25	-3.112 ± 0.965	**0.007**	-2.746 ± 0.886	**0.009**	-1.836 ± 0.904	0.089

Legend: IR = Inner Retina; ONL = Outer Nuclear Layer; IS = Photoreceptor Inner Segment; OS = Photoreceptor Outer Segment; RPE = Retinal Pigment Epithelium; TR = Total Retina; Bold: Progression is statistically significant ($p<0.05$)

3.2.3 Baseline values of the intact area

The baseline values of the intact area of the IR were 0.78 (SD±0) mm^2, of the ONL 0.72 (±0.22) mm^2, of the IS 0.25 (SD±0.37) mm^2, of the OS 0.2 (SD±0.32) mm^2, of the RPE 0.42 (SD±0.38) $mm^2$and of the TR 0.78 (SD±0.01) mm^2 (Table 3).

3.2.4 Intact area – estimated yearly rate difference in progression

The estimated yearly rate difference of the IR showed a change of 0.001 (SD±0.001) mm^2, of the ONL 0.002 (SD±0.003) mm^2, of the IS 0.001 (SD±0.002) mm^2, of the OS -0.008 (SD±0.009) mm^2, of the RPE -0.033 (SD±0.017) mm^2 and of the TR 0.001 (SD±0.001) mm^2 (Table 3).

Table 3: Estimated annual growth rates in the central subfield, the inner ring and the outer ring of the progression of atrophy of the intact area [mm^2 per year] of the examined retinal layers.

Adapted from Grosspoetzl et al. with permission of Elsevier under the terms of the Creative Commons CC-BY license (1).

Retinal layers	**Baseline values of the intact area [mm^2], mean ± standard deviation**			**Estimated rate difference in progression [mm^2 per year] of the intact area, coefficient ± standard error; p-value**					
	Central subfield	**Inner ring**	**Outer ring**	**Central subfield**	**p-value**	**Inner ring**	**p-value**	**Outer ring**	**p-value**
IR	0.78 ± 0.00	6.28 ± 0.01	20.91 ± 0.41	0.001 ± 0.001	1.000	0.001 ± 0.001	0.585	-0.019 ± 0.017	0.297
ONL	0.72 ± 0.22	6.05 ± 0.74	20.87 ± 0.45	0.002 ± 0.003	0.387	-0.050 ± 0.056	0.392	-0.062 ± 0.017	**0.011**
IS	0.25 ± 0.37	2.22 ± 2.47	14.93 ± 7.69	0.001 ± 0.002	0.673	-0.114 ± 0.005	**0.043**	-0.609 ± 0.276	0.070
OS	0.20 ± 0.32	1.13 ± 1.77	11.96 ± 8.40	-0.008 ± 0.009	0.346	-0.194 ± 0.137	0.181	-0.609 ± 0.293	0.083
RPE	0.42 ± 0.38	4.44 ± 2.29	20.01 ± 2.23	-0.033 ± 0.017	0.085	-0.397 ± 0.132	**0.011**	-0.413 ± 0.241	0.138
TR	0.78 ± 0.01	6.28 ± 0.01	20.91 ± 0.41	0.001 ± 0.001	1.000	0.001 ± 0.001	0.585	-0.019 ± 0.017	0.299

Legend: IR = Inner Retina; ONL = Outer Nuclear Layer; IS = Photoreceptor Inner Segment; OS = Photoreceptor Outer Segment; RPE = Retinal Pigment Epithelium; TR = Total Retina; Bold: Progression is statistically significant ($p<0.05$)

3.2.5 Intact area – estimated yearly rate difference in progression determined by the square root

The estimated yearly rate difference determined by the square root revealed a progression of 0.001 (SD±0.001) mm in the IR, of 0.001 (SD±0.001) mm in the ONL, of -0.003 (SD±0.006) mm in the IS, of 0.004 (SD±0.011) mm in the OS, of -0.03 (SD±0.013) mm in the RPE and of 0.001 (SD±0.001) mm in the TR).

The estimated difference in progression determined by the square root revealed statistically significant decline in the RPE (p=0.04) (Table 4).

Table 4: Estimated annual growth rates in the central subfield, the inner ring and the outer ring of the progression of effective lesion radius [mm per year], determined from the square root (lesion area /π) for the intact area.

Adapted from Grosspoetzl et al. with permission of Elsevier under the terms of the Creative Commons CC-BY license (1).

Estimated rate difference in progression [mm per year] of the effective lesion radius determined by the square root, coefficient ± standard error; p-value						
	Central subfield	**p-value**	**Inner ring**	**p-value**	**Outer ring**	**p-value**
IR	0.001 ± 0.001	1.000	0.001 ± 0.001	0.584	-0.002 ± 0.002	0.296
ONL	0.001 ± 0.001	0.387	-0.015 ± 0.017	0.373	-0.007 ± 0.002	**0.011**
IS	-0.003 ± 0.006	0.605	-0.067 ± 0.027	**0.031**	-0.123 ± 0.061	0.090
OS	0.004 ± 0.011	0.741	-0.064 ± 0.087	0.283	-0.067 ± 0.087	0.469
RPE	-0.030 ± 0.013	**0.040**	-0.128 ± 0.034	**0.003**	-0.053 ± 0.034	0.168
TR	0.001 ± 0.001	1.000	0.001 ± 0.001	0.584	-0.002 ± 0.002	0.296

Legend: IR = Inner Retina; ONL = Outer Nuclear Layer; IS = Photoreceptor Inner Segment; OS = Photoreceptor Outer Segment; RPE = Retinal Pigment Epithelium; TR = Total Retina; Bold: Progression is statistically significant ($p<0.05$)

3.3 Inner Ring of the ETDRS grid

The inner Ring of the ETDRS grid is a distinct and essential component of retinal imaging and analysis. This region, encompassing a diameter of 1.5mm to 0.5mm around the anatomical fovea, holds a prominent place in ophthalmology and clinical research. Within the inner Ring, the intricate layers of the retina are meticulously examined, with a specific focus on thickness measurements and the presence of atrophy.

Changes in thickness and integrity within the inner Ring provides critical insights into the progression of STGD4.

3.3.1 Mean thickness baseline

At the baseline visit the mean thickness of the IR was 141.29 (SD±21.02) µm, of the ONL 42.44 (SD±15.67) µm, of the IS 7.18 (SD±10.82) µm, of the OS 1.38 (SD±3.15) µm, of the RPE 14.35 (SD±9.1) µm and of the TR 222.11 (SD±34.77) µm (Table 2).

3.3.2 Mean thickness - estimated yearly rate difference

The estimated yearly rate difference of the IR showed -0,542 (SD±0.062) µm, of the ONL -1.108 (SD±0.651) µm, of the IS -0.6 (SD±0.288) µm, of the OS -0.135 (SD±0.093) µm, of the RPE -1.939 (SD±0.511) µm and of the TR -2.746 (SD±0.886) µm.
The mean RPE thickness and the mean TR thickness decreased significantly during the 24 months observation (all $p<0,05$) (Table 2).

3.3.3 Baseline values of the intact area

The baseline values of the intact area of the IR were 6.28 (SD±0.01) mm^2, of the ONL 6.05 (±0.74) mm^2, of the IS 2.22 (SD±2.47) mm^2, of the OS 1.13 (SD±1.77) mm^2, of the RPE 4.44 (SD±2.29) mm^2 and of the TR 6.28 (SD±0.01) mm^2 (Table 3).

3.3.4 Intact area – estimated yearly rate difference in progression

The estimated yearly rate difference of the IR showed a change of 0.001 (SD±0.001) mm^2, of the ONL -0.05 (SD±0.056) mm^2, of the IS -0.114 (SD±0.005) mm^2, of the OS -0.194 (SD±0.137) mm^2, of the RPE -0.397 (SD±0.132) mm^2 and of the TR 0.001 (SD±0.001) mm^2.
The estimated yearly rate difference in progression revealed statistically significancy in the IS and the RPE (all $p<0.05$) (Table 3).

3.3.5 Intact area – estimated yearly rate difference in progression determined by the square root

The estimated yearly rate difference determined by the square root revealed a progression of 0.001 (SD±0.001) mm per year in the IR, of -0.015 (SD±0.017) mm per year in the ONL, of -0.067 (SD±0.027) mm per year in the IS, of -0.064 (SD±0.087) mm per year in the OS, of -0.128 (SD±0.034) mm per year in the RPE and of 0.001 (SD±0.001) mm per year in the TR).
The estimated difference in progression determined by the square root revealed statistically significant decline in the IS and the RPE ($p<0.05$) (Table 4).

3.4 Outer Ring of the ETDRS grid

The Outer Ring of the ETDRS grid plays a crucial part in retinal imaging and clinical analysis. Spanning from 3mm to 1.5mm away from the anatomical fovea, this region serves as a vital extension of the grid, encompassing a broader field of the retina. Within the Outer Ring, the retinal layers are subjected to meticulous scrutiny, with a specific emphasis on thickness measurements and atrophy.

This extended area plays a pivotal role in comprehensive retinal assessment, often providing insights into the progression of retinal diseases that extend beyond the central subfield and inner Ring.

It is important to acknowledge that in 6 of the 13 eyes in our study, the eye tracking option could not be applied during the follow-up period. Consequently, the cube scan covered different retinal locations concerning the outer ring, which may introduce nuances in our analysis. Nevertheless, 7 eyes with consistent imaging of the same retinal regions were included in the analysis of the outer ring.

3.4.1 Mean thickness at baseline

The mean thickness of the IR was 132.96 (SD±12.70) µm, of the ONL 49.41 (SD±16.62) µm, of the IS 19.71 (SD±15.19) µm, of the OS 4.91 (SD±4.63) µm, of the RPE 20.67 (SD±4.6) µm and of the TR 232.6 (SD±34.25) µm (Table 2).

3.4.2 Mean thickness - estimated yearly rate difference

The estimated yearly rate difference of the IR showed a decline of -0.029 (SD±0.07) µm, of the ONL -1.55 (SD±0.481) µm, of the IS -0.714 (SD±0.238) µm, of the OS -0.307 (SD±0.145) µm, of the RPE -1.321 (SD±0.917) µm and of the TR -1.836 (SD±0.904) µm.

The mean thickness of the ONL the IS showed statistically significant decline after 24 months (all $p<0.05$) (Table 2).

3.4.3 Baseline values of the intact area

The baseline values of the intact area of the IR were 20.91 (SD±0.41) mm^2, of the ONL 20.87 (±0.45) mm^2, of the IS 14.93 (SD±7.69) mm^2, of the OS 11.96 (SD±8.4) mm^2, of the RPE 20.01 (SD±2.23) mm^2 and of the TR 20.91 (SD±0.41) mm^2 (Table 3).

3.4.4 Intact area – estimated yearly rate difference in progression

The estimated yearly rate difference of the IR showed a change of -0.019 (SD±0.017) mm^2, of the ONL -0.062 (SD±0.017) mm^2, of the IS -0.609 (SD±0.276) mm^2, of the OS -0.609 (SD±0.293) mm^2, of the RPE -0.413 (SD±0.241) mm^2 and of the TR -0.019 (SD±0.017) mm^2. The estimated yearly rate difference in progression of the intact area showed statistically significance of the ONL (p=0.011) (Table 3).

3.4.5 Intact area – estimated yearly rate difference in progression determined by the square root

The estimated yearly rate difference determined by the square root revealed a progression of -0.002 (SD±0.002) mm per year in the IR, of -0.007 (SD±0.002) mm per year in the ONL, of -0.123 (SD±0.061) mm per year in the IS, of -0.067 (SD±0.087) mm per year in the OS, of -0.053 (SD±0.034) mm per year in the RPE and of -0.02 (SD±0.002) mm per year in the TR). The estimated difference in progression determined by the square root revealed statistically significant change in the ONL (p=0.011) (Table 4).

4 Discussion

The application of SD-OCT in retinal imaging has represented a transformative leap in our understanding of the pathophysiological intricacies underpinning retinal degenerations. These conditions frequently culminate in the demise of photoreceptor and RPE cells, a process notoriously intricate and challenging to decipher. In particular, the ability of SD-OCT to resolve the photoreceptor bands and deliver high-resolution imaging has been previously expounded upon, highlighting the invaluable advantages it offers in assessing atrophic regions of the retina. The precision, safety, and enhanced patient comfort inherent in SD-OCT imaging are well-documented attributes that have bolstered its prominence in the field of retinal research. Beyond these inherent merits, SD-OCT carries the promise of potentially serving as a surrogate endpoint in upcoming clinical trials. This prospect is of paramount importance, as it can significantly expedite the evaluation of novel therapeutic interventions targeting retinal degenerations. The ability to discern and quantify changes in photoreceptor and RPE integrity, in conjunction with the precise evaluation of atrophic regions, renders SD-OCT a pivotal tool in unravelling the pathogenesis of these conditions and assessing the efficacy of potential treatments. Consequently, the utilization of SD-OCT holds profound implications for advancing our knowledge of retinal pathophysiology and hastening the development of therapeutic strategies aimed at preserving retinal function and vision in STGD4 (8).

In this research endeavour, we aim to present the inaugural prospective cohort investigation into structural modifications associated with *PROM1*-associated retinal degeneration by leveraging SD-OCT. Our study represents a pioneering effort to shed light on the pathophysiological processes of this condition. Our comprehensive analysis yielded compelling findings, marked by statistically significant reductions in the mean thickness of the RPE and the TR within both the CS and the inner ring. Furthermore, our investigations unveiled statistically significant decreases in the thickness of the ONL and the IS within the outer ring. Notably, we also documented a noteworthy reduction in the intact area of the RPE and IS within the inner ring and a decrease in the intact area of the ONL within the outer ring. These findings collectively underscore the progressive nature of structural alterations in *PROM1*-associated retinal degeneration, painting a clear picture of the diminishing macular thickness and a

concurrent reduction in intact areas throughout various retinal layers over a 24-month observational timeframe. Our novel insights hold significant implications for the understanding and monitoring of *PROM1*-associated retinal degeneration, potentially guiding future interventions aimed at preserving retinal structure and function in affected individuals.

SD-OCT was selected as a secondary endpoint in the ProgStar trials involving *ABCA4*-associated STGD1 (87) and subsequently, it was also incorporated as a secondary endpoint in the ProgStar-4 study, where fundus autofluorescence served as the primary endpoint. It has been documented that the integrity of the EZ in STGD1 patients exhibits correlations with variations in visual acuity, microperimetry sensitivity, the extent of fundus lesions, and mfERG outcomes. Consequently, the evaluation of the EZ emerges as a particularly crucial parameter in the context of STGD1 (88,89). Another study established a direct correlation between visual acuity and the volume of the EZ/OS while inversely correlating it with en face EZ loss/atrophy and OS/EZ attenuation (90).

Despite the common terminology, significant disparities exist between STGD1 and STGD4. Notably, in individuals afflicted with STGD4, an intriguing clinical observation has been made, indicating that the disease may initially manifest in a localized manner, primarily affecting the macular region. This initial presentation is characterized by distinctive features, including an augmented foveal reflex and a peculiar red-speckled appearance within the macula. Over the course of the disease progression, these early clinical signs evolve into a distinctive bull's-eye maculopathy pattern. As time elapses, this bull's-eye configuration ultimately gives way to the development of macular atrophy, reflecting the relentless degeneration of the macular structure. This particular disease course in STGD4, characterized by its localized and evolving nature, underscores the unique clinical nuances associated with this subtype of Stargardt disease, distinct from the more widely recognized STGD1. Such insights into the differential disease trajectories are instrumental in enhancing our understanding of these conditions and are pivotal in guiding both diagnosis and management strategies for affected patients. (31). Nonetheless, despite considerable research efforts, the intricate and nuanced underlying mechanisms responsible for the pathogenesis of this condition remain incompletely understood. The hallmark clinical presentation, which often manifests as ring-shaped RPE atrophy with an intact foveal center, has garnered significant attention in the field of retinal degenerative diseases. A

prevailing hypothesis posits that this distinct clinical pattern can be linked to the progressive accumulation of lipofuscin within the RPE cells. Lipofuscin, a byproduct of photoreceptor outer segment metabolism, is particularly conspicuous in its accumulation at the posterior pole of the retina. (91,92). As the disease progresses, the foveal center also becomes affected (31).

Studies have indicated that *PROM1* is essential for maintaining the expression levels of *ABCA4* and *RDH12*. This suggests that *PROM1* may play a role in regulating the visual cycle, particularly in the conversion of all-trans-retinal to all-trans-retinol (81). Alternatively, *PROM1* may indirectly influence lipofuscin accumulation through *ABCA4* dysfunction, which could result from disruptions in the outer segment structure (93,94). These changes are consistent with the findings of our study, where we observed that the RPE of the inner ring and the central subfield were particularly affected by atrophy. In our study, two SD-OCT-derived variables hold potential as surrogate endpoints: changes in mean retinal thickness and changes in intact area (i.e., thickness > 0 µm at baseline). While changes in mean retinal thickness may exhibit only minor differences over time (also, depending on grading protocols (95)), the change in intact area can provide more robust parameters. However, it is worth noting that changes in intact area may depend on the initial lesion size. To account for this, we used the square root of the area's radius to better represent the increase in atrophy, as significant differences existed in our patient population concerning the initial size of the intact area. This square root transformation of lesion area measurements has previously been employed in patients with geographic atrophy in age-related macular degeneration to eliminate the dependency of growth rates on the original lesion size (96). This approach can simplify the design and enrolment in clinical trials, as there may be no need to specify a range of lesion sizes or include lesion size in the analysis (96).

Inherited macular and retinal dystrophies constitute a well-established category of debilitating ocular disorders characterized by a progressive deterioration of both retinal function and structural integrity. These conditions collectively share a common feature of degenerative changes within the macular and retinal regions, resulting in a gradual and often irreversible loss of vision. While the general trajectory of retinal degeneration in these disorders is widely recognized, it is imperative to acknowledge the remarkable degree of heterogeneity that prevails in the rate of disease progression. This variability manifests not only among individual patients

but also within specific familial groups. This inherent diversity in progression dynamics represents a multifaceted and intriguing facet of inherited retinal dystrophies (28,31,97,98). Understanding the underlying factors contributing to the variable progression of retinal dystrophies stands as a pivotal frontier in the ongoing quest for improved patient care and therapeutic strategies. While the fundamental mechanisms of disease pathogenesis are broadly recognized, the specific attributes of variable progression remain an area of intense investigation, one that promises to yield valuable insights to enhance our ability to manage and eventually mitigate the impact of these conditions on affected individuals and their families. In the course of our investigation, we meticulously tracked the changes in various retinal layers over a span of 24 months, revealing a discernible decline in these retinal components. It is noteworthy that, while these alterations were evident, we only managed to establish statistical significance in specific subretinal layers and particular regions of the retina. This nuanced outcome can be attributed to several factors, which warrant careful consideration. First and foremost, it is crucial to underscore that *PROM1*-associated retinal degeneration typically follows a gradual and protracted disease course. This progressive nature is intrinsic to the condition and, further complicating our analysis, the precise onset age of the disease within our cohort of patients remained uncertain. Given this inherent variability and the characteristic slow progression of *PROM1*-associated retinal degeneration, it is plausible that a 24-month observation period might not have been sufficiently comprehensive to capture significant and widespread changes across all retinal layers and regions. Despite these challenges, it is vital to recognize the pioneering nature of our study. To the best of our knowledge, our investigation represents the inaugural attempt to systematically monitor retinal thicknesses and the extent of intact retinal areas in patients afflicted *PROM1*-associated retinal degeneration over a 24-month timeframe. This endeavour has contributed invaluable insights into the natural history of the disease, even though we acknowledge the potential limitations imposed by the relatively short observation period and the intrinsic heterogeneity in disease progression. Our findings constitute a critical stepping stone for future research aimed at comprehending the dynamics of *PROM1*-associated retinal degeneration, with the ultimate goal of advancing diagnostic and therapeutic strategies to mitigate its impact on affected individuals.

The evaluation and categorization of atrophy in STGD4 using SD-OCT has posed significant challenges. The software algorithm employed often resulted in errors, primarily due to the

presence of hyperreflective debris in atrophic areas, which is more common in STGD4 compared to dry age-related macular degeneration. Consequently, substantial manual corrections were required (99). Similar challenges were observed in a preliminary study involving *ABCA4*-related STGD1, where misidentification of the outer retina occurred in up to 20.2% of B-scans, and over 30% of B-scans exhibited notable software errors (100). Furthermore, an initial analysis of the repeatability of SD-OCT grading demonstrated significant noise in the assessment of the RPE. There was substantial variability between gradings, as evidenced by poor intra-class correlations and high relative absolute differences (RADs) in thickness and intact area measurements. However, measurements of thickness and intact area in the inner and outer segments of the inner and outer ring regions displayed good to excellent intra-class correlations (95). Additionally, the phenotypes observed in this study of *PROM1*-related STGD4 exhibited a highly heterogeneous appearance, dependent on the specific disease stage. This further complicated the utilization, examination, and quantification of SD-OCT images.

When endeavouring to interpret the data related to disease progression, it is imperative to maintain a clear understanding of the various factors that can influence the results. The measurements of retinal thicknesses and intact areas, while informative, are inherently subject to notable variability, which can be attributed to a range of sources, such as inherent measurement imprecision, individual anatomical differences, and variability in disease manifestation. As a result, it is important to exercise caution when relying solely on these metrics as primary indicators of disease progression. In this context, it is prudent to consider the suitability of these measurements as outcome measures for specific subtypes of retinal atrophy, where the manifestations are more predictable and uniform. In such cases, changes in retinal thicknesses and intact areas may provide valuable insights into the progression of the disease. However, in the broader context of assessing disease progression, there is merit in exploring alternative and potentially more reliable outcome measures. In particular, directing attention towards structural elements like the IS and OS layers, including the EZ, holds promise. These structures are of particular interest due to their critical roles in maintaining photoreceptor integrity and function, and alterations in these regions may offer more robust and clinically relevant markers of disease progression in various retinal degenerative conditions. Thus, the complexity and variability of the data underscore the importance of employing a multifaceted

approach to comprehensively evaluate disease progression in retinal disorders. This approach may involve considering a combination of retinal thickness measurements and structural changes in specific retinal layers to provide a more accurate representation of the evolving disease process. Longitudinal data rely on consistent measurement locations. Despite the imaging protocol of ProgStar-4, which required photographers to align the 20° x 20° cube scan with the anatomical fovea and utilize the follow-up and eye-tracking functions of the Heidelberg Spectralis device, patients often exhibited eccentric fixation due to preexisting or developing atrophy. Consequently, the cube scan could not always be perfectly centered on the anatomical fovea, or it might have led to the development of a new preferred retinal locus. As a result, some portions of the outer EDTRS ring were either missing at baseline or during follow-up, necessitating their exclusion from the analysis (101).

While our research adopts a multicenter design and aims to offer a comprehensive analysis of *PROM1*-associated retinal degenerations, it is essential to recognize and carefully address certain limitations inherent in the study, which may impact the generalizability and interpretation of the findings. One notable limitation pertains to the relatively small number of cases included in our study. This constraint is primarily attributable to the rarity of *PROM1*-associated retinal degenerations, which were genuinely infrequent at the time of study inception. As such, the study was inherently constrained by the limited availability of affected individuals for participation, which, in turn, influenced the sample size. This scarcity of cases might entail potential implications for the statistical robustness and generalizability of the study's findings. Another constraint worthy of attention pertains to the challenge of ascertaining the precise disease stage of each individual patient within the cohort. The dynamic nature of retinal degenerative conditions like *PROM1*-associated retinal degenerations complicates the classification of patients into specific disease stages, and this variability can introduce ambiguity in data interpretation. To mitigate this limitation, we implemented a square root calculation to assess the dimensions of atrophic lesions and intact areas, aiming to capture a more nuanced understanding of the disease's structural changes.
Nevertheless, it is vital to acknowledge that these limitations might introduce certain degrees of variability and uncertainty into our findings, particularly when considering the mean thickness measurements of individual retinal layers under scrutiny. The sample size constraints and the challenge of precisely defining disease stages are factors that potentially impact the

accuracy and robustness of the measurements, necessitating a cautious approach when drawing conclusions from the data. There is a need for continued efforts to expand sample sizes and refine methodologies to further advance our comprehension of *PROM1*-associated retinal degenerations and other rare disorders, ultimately contributing to the development of more effective diagnostic and therapeutic strategies.

However, SD-OCT offers a multitude of advantages, rendering it a promising choice for potential surrogate outcome measures in forthcoming clinical trials. This imaging modality provides the distinct advantage of non-invasiveness, allowing for swift assessments, in stark contrast to procedures such as microperimetry. Moreover, these assessments can be standardized consistently across different study sites, mitigating potential variations in data acquisition and reducing the risk of retinal light toxicity, a concern often associated with FAF (102). Furthermore, SD-OCT affords the unique capability of visualizing photoreceptors or their subcomponents, rendering it a viable candidate for consideration by regulatory authorities as a surrogate endpoint (83). This attribute holds significant promise for enhancing the sensitivity and specificity of clinical trials, potentially expediting the development and approval of novel therapeutic interventions.

SD-OCT emerges as a particularly well-suited diagnostic tool, demonstrating its efficacy primarily during the nascent stages of retinal diseases. This diagnostic power is most pronounced when patients maintain stable fixation, and the pathological changes are primarily confined to the central macular region. During this early phase of the disease, the notable alterations primarily manifest within the IS/OS or EZ of the photoreceptor layer, rather than in the RPE. This distinction underscores the pivotal role that SD-OCT plays in characterizing the early stages of retinal pathologies. In fact, one of the research groups affiliated with our multicenter study embarked on an in-depth phenotyping investigation, which encompassed four patients featured in our report. Their dedicated efforts and findings yielded compelling evidence suggesting that FAF, another imaging modality frequently employed in retinal disease research, may possess notable limitations in capturing the nuances of the disease during its initial phases. Conversely, the study findings affirmed the robustness and reliability of SD-OCT as a critical tool for effectively monitoring disease progression in these early stages. This demonstrates the distinct advantage of SD-OCT over other imaging techniques, offering clinicians and

researchers a reliable means of tracking the disease dynamics and, consequently, guiding more informed diagnostic and therapeutic decisions. The insights from this research collectively contribute to a deeper understanding of the potential diagnostic strengths of SD-OCT and the relative limitations of alternative methods, underscoring the significance of tailored diagnostic approaches in the management of retinal diseases.(103).

A plausible and compelling inference can be drawn regarding the patients who exhibit discernible alterations within their retinal layers in the early stages of the disease. Such individuals may represent a particularly promising subset of candidates for pharmaceutical or gene therapy interventions, specially designed to safeguard the remaining photoreceptor and/or RPE cells, or to stave off the relentless progression of degeneration in these cells. The rationale underlying this assumption is rooted in the observed structural changes within the retinal layers, as evidenced by techniques such as SD-OCT. When these alterations manifest, it often signifies an advanced stage of the disease process, with a significant burden of cell damage and loss already incurred. As a result, the urgency of therapeutic intervention becomes paramount in an effort to halt or mitigate further deterioration and to potentially rescue the surviving photoreceptors and RPE cells. Pharmaceutical or gene-based therapies have shown promise in the context of retinal degenerative diseases by aiming to either slow the degenerative process or promote cellular survival. Patients at an earlier stage of retinal degeneration, where these therapeutic strategies may have a more profound impact on preserving vision, could stand to benefit substantially. This inference underscores the potential for tailored treatment strategies that consider the specific structural and clinical characteristics of individual patients. By doing so, it paves the way for precision medicine approaches that hold the promise of improved outcomes for those grappling with retinal degenerations. Consequently, the identification and monitoring of these structural changes through advanced imaging technologies assume greater significance, ultimately guiding the development of targeted therapies and enhancing the quality of care for affected individuals (104).

Further investigations of a more extensive nature and depth are indispensable to discern and establish robust correlations between the observed structural alterations in retinal layers and the associated visual function parameters. This exploration would ideally encompass a comprehensive range of visual function assessments, including photopic and scotopic

microperimetry, two fundamental techniques for evaluating the functional attributes of the human visual system. The envisioned research would go beyond the mere recognition of structural changes and delve into the intricate interplay between these anatomical modifications and the actual functional implications they bear on an individual's vision. Photopic microperimetry, tailored to evaluate visual function under well-lit conditions, and scotopic microperimetry, designed for low-light or dark-adapted settings, provide nuanced insights into how the retina responds to varying levels of illumination. By scrutinizing and quantifying the interrelationships between structural changes and the parameters gauged by these advanced visual function assessments, a more comprehensive understanding of the disease process would emerge. Such a multifaceted approach would furnish invaluable insights into the complex dynamics at play in retinal pathologies and, in particular, how they manifest in individual patients. Additionally, it would offer a solid foundation for tailoring therapeutic strategies and intervention approaches that effectively target the underlying mechanisms of retinal degenerations, ultimately optimizing visual outcomes and enhancing patients' quality of life. In essence, this calls for a multidisciplinary collaboration between ophthalmologists and researchers, leveraging the full spectrum of clinical and research tools to uncover the intricate relationships between structural changes and visual function parameters, forging a path towards more effective treatments and improved patient care in the realm of retinal disorders (97,105).

5 References

1. Grosspoetzl M, Riedl R, Schliessleder G, Hu ZJ, Michaelides M, Sadda S, u. a. The Progression of PROM1-associated retinal degeneration as determined by spectral-domain optical coherence tomography over a 24-months period. American Journal of Ophthalmology. November 2023;S0002939423004725.

2. Allikmets R, Singh N, Sun H, Shroyer NF, Hutchinson A, Chidambaram A, u. a. A photoreceptor cell-specific ATP-binding transporter gene (ABCR) is mutated in recessive Starqardt macular dystrophy. Nat Genet. 1. März 1997;15(3):236–46.

3. Tsang SH, Sharma T. Stargardt Disease. In: Tsang SH, Sharma T, Herausgeber. Atlas of Inherited Retinal Diseases [Internet]. Cham: Springer International Publishing; 2018 [zitiert 6. Juni 2022]. S. 139–51. (Advances in Experimental Medicine and Biology; Bd. 1085). Verfügbar unter: http://link.springer.com/10.1007/978-3-319-95046-4_27

4. Kong X, Fujinami K, Strauss RW, Munoz B, West SK, Cideciyan AV, u. a. Visual Acuity Change Over 24 Months and Its Association With Foveal Phenotype and Genotype in Individuals With Stargardt Disease. JAMA Ophthalmol. August 2018;136(8):920–8.

5. Tanna P, Strauss RW, Fujinami K, Michaelides M. Stargardt disease: clinical features, molecular genetics, animal models and therapeutic options. Br J Ophthalmol. Januar 2017;101(1):25–30.

6. Van Huet RAC, Bax NM, Westeneng-Van Haaften SC, Muhamad M, Zonneveld-Vrieling MN, Hoefsloot LH, u. a. Foveal Sparing in Stargardt Disease. Invest Ophthalmol Vis Sci. 21. November 2014;55(11):7467.

7. Schönbach EM, Ibrahim MA, Strauss RW, Birch DG, Cideciyan AV, Hahn GA, u. a. Fixation Location and Stability Using the MP-1 Microperimeter in Stargardt Disease. Ophthalmology Retina. Januar 2017;1(1):68–76.

8. Cideciyan AV, Swider M, Aleman TS, Sumaroka A, Schwartz SB, Roman MI, u. a. *ABCA4* -Associated Retinal Degenerations Spare Structure and Function of the Human Parapapillary Retina. Invest Ophthalmol Vis Sci. 1. Dezember 2005;46(12):4739.

9. Cremers FPM, Lee W, Collin RWJ, Allikmets R. Clinical spectrum, genetic complexity and therapeutic approaches for retinal disease caused by ABCA4 mutations. Progress in Retinal and Eye Research. November 2020;79:100861.

10. Heath Jeffery RC, Mukhtar SA, McAllister IL, Morgan WH, Mackey DA, Chen FK. Inherited retinal diseases are the most common cause of blindness in the working-age population in Australia. Ophthalmic Genetics. 4. Juli 2021;42(4):431–9.

11. Szlyk JP, Fishman GA, Grover S, Revelins BI, Derlacki DJ. Difficulty in performing everyday activities in patients with juvenile macular dystrophies: comparison with

patients with retinitis pigmentosa. British Journal of Ophthalmology. 1. Dezember 1998;82(12):1372–6.

12. Beck RW, Maguire MG, Bressler NM, Glassman AR, Lindblad AS, Ferris FL. Visual Acuity as an Outcome Measure in Clinical Trials of Retinal Diseases. Ophthalmology. Oktober 2007;114(10):1804–9.

13. Piotter E, McClements ME, MacLaren RE. Therapy Approaches for Stargardt Disease. Biomolecules. 9. August 2021;11(8):1179.

14. Stargardt K. Über familiäre, progressive Degeneration in der Maculagegend des Auges. Graefes Arhiv für Ophthalmologie. September 1909;71(3):534–50.

15. Klien BA, Krill AE. Fundus flavimaculatus. Clinical, functional and histopathologic observations. Am J Ophthalmol. Juli 1967;64(1):3–23.

16. François P, Turut P, Puech B, Hache JC. [Stargardt's disease and fundus flavimaculatus]. Arch Ophtalmol Rev Gen Ophtalmol. November 1975;35(11):817–46.

17. Fishman GA. Fundus flavimaculatus. A clinical classification. Arch Ophthalmol. Dezember 1976;94(12):2061–7.

18. Kim LS, Fishman GA. Comparison of Visual Acuity Loss in Patients with Different Stages of Stargardt's Disease. Ophthalmology. Oktober 2006;113(10):1748–51.

19. Papermaster DS, Converse CA, Zorn M. Biosynthetic and immunochemical characterization of large protein in frog and cattle rod outer segment membranes. Exp Eye Res. August 1976;23(2):105–15.

20. Anderson KL, Baird L, Lewis RA, Chinault AC, Otterud B, Leppert M, u. a. A YAC contig encompassing the recessive Stargardt disease gene (STGD) on chromosome 1p. Am J Hum Genet. Dezember 1995;57(6):1351–63.

21. Gerber S, Rozet JM, Bonneau D, Souied E, Camuzat A, Dufier JL, u. a. A gene for late-onset fundus flavimaculatus with macular dystrophy maps to chromosome 1p13. Am J Hum Genet. Februar 1995;56(2):396–9.

22. Lambertus S, van Huet RAC, Bax NM, Hoefsloot LH, Cremers FPM, Boon CJF, u. a. Early-Onset Stargardt Disease. Ophthalmology. Februar 2015;122(2):335–44.

23. Edwards AO, Donoso LA, Ritter R. A novel gene for autosomal dominant Stargardt-like macular dystrophy with homology to the SUR4 protein family. Invest Ophthalmol Vis Sci. Oktober 2001;42(11):2652–63.

24. Zhang K, Kniazeva M, Han M, Li W, Yu Z, Yang Z, u. a. A 5-bp deletion in ELOVL4 is associated with two related forms of autosomal dominant macular dystrophy. nature genetics. 2001;27.

25. Kniazeva M, Chiang MF, Morgan B, Anduze AL, Zack DJ, Han M, u. a. A New Locus for Autosomal Dominant Stargardt-Like Disease Maps to Chromosome 4. The American Journal of Human Genetics. Mai 1999;64(5):1394–9.

26. Corbeil D, Röper K, Fargeas CA, Joester A, Huttner WB. Prominin: A Story of Cholesterol, Plasma Membrane Protrusions and Human Pathology: Prominin and Plasma Membrane Protrusions. Traffic. Januar 2001;2(2):82–91.

27. Weigmann A, Corbeil D, Hellwig A, Huttner WB. Prominin, a novel microvilli-specific polytopic membrane protein of the apical surface of epithelial cells, is targeted to plasmalemmal protrusions of non-epithelial cells. Proc Natl Acad Sci USA. 11. November 1997;94(23):12425–30.

28. Zhang Q, Zulfiqar F, Xiao X, Riazuddin SA, Ahmad Z, Caruso R, u. a. Severe retinitis pigmentosa mapped to 4p15 and associated with a novel mutation in the PROM1 gene. Hum Genet. November 2007;122(3–4):293–9.

29. Maw MA, Corbeil D, Koch J, Hellwig A, Wilson-Wheeler JC, Bridges RJ, u. a. A frameshift mutation in prominin (mouse)-like 1 causes human retinal degeneration. Human Molecular Genetics. 1. Januar 2000;9(1):27–34.

30. Yang Z, Chen Y, Lillo C, Chien J, Yu Z, Michaelides M, u. a. Mutant prominin 1 found in patients with macular degeneration disrupts photoreceptor disk morphogenesis in mice. J Clin Invest. 1. Juli 2008;JCI35891.

31. Michaelides M, Gaillard MC, Escher P, Tiab L, Bedell M, Borruat FX, u. a. The *PROM1* Mutation p.R373C Causes an Autosomal Dominant Bull's Eye Maculopathy Associated with Rod, Rod–Cone, and Macular Dystrophy. Invest Ophthalmol Vis Sci. 1. September 2010;51(9):4771.

32. Maw MA. A frameshift mutation in prominin (mouse)-like 1 causes human retinal degeneration. Human Molecular Genetics. 1. Januar 2000;9(1):27–34.

33. Cehajic-Kapetanovic J, Birtel J, McClements ME, Shanks ME, Clouston P, Downes SM, u. a. Clinical and Molecular Characterization of *PROM1* -Related Retinal Degeneration. JAMA Netw Open. 14. Juni 2019;2(6):e195752.

34. Curtis HJ, Seow Y, Wood MJA, Varela MA. Knockdown and replacement therapy mediated by artificial mirtrons in spinocerebellar ataxia 7. Nucleic Acids Research. 27. Juli 2017;45(13):7870–85.

35. Cehajic-Kapetanovic J, Eleftheriou C, Allen AE, Milosavljevic N, Pienaar A, Bedford R, u. a. Restoration of Vision with Ectopic Expression of Human Rod Opsin. Current Biology. August 2015;25(16):2111–22.

36. Rattner A, Smallwood PM, Williams J, Cooke C, Savchenko A, Lyubarsky A, u. a. A Photoreceptor-Specific Cadherin Is Essential for the Structural Integrity of the Outer Segment and for Photoreceptor Survival. Neuron. Dezember 2001;32(5):775–86.

37. Rattner A, Chen J, Nathans J. Proteolytic Shedding of the Extracellular Domain of Photoreceptor Cadherin. Journal of Biological Chemistry. Oktober 2004;279(40):42202–10.

38. Lewis RG, Simpson B. Genetics, Autosomal Dominant. In: StatPearls [Internet]. Treasure Island (FL): StatPearls Publishing; 2023 [zitiert 24. August 2023]. Verfügbar unter: http://www.ncbi.nlm.nih.gov/books/NBK557512/

39. Panoutsopoulou K, Wheeler E. Key Concepts in Genetic Epidemiology. In: Evangelou E, Herausgeber. Genetic Epidemiology [Internet]. New York, NY: Springer New York; 2018 [zitiert 24. August 2023]. S. 7–24. (Methods in Molecular Biology; Bd. 1793). Verfügbar unter: http://link.springer.com/10.1007/978-1-4939-7868-7_2

40. Huckfeldt RM, East JS, Stone EM, Sohn EH. Phenotypic Variation in a Family With Pseudodominant Stargardt Disease. JAMA Ophthalmol. 1. Mai 2016;134(5):580.

41. Huang WC, Cideciyan AV, Roman AJ, Sumaroka A, Sheplock R, Schwartz SB, u. a. Inner and Outer Retinal Changes in Retinal Degenerations Associated With *ABCA4* Mutations. Invest Ophthalmol Vis Sci. 20. März 2014;55(3):1810.

42. Khan KN, Kasilian M, Mahroo OAR, Tanna P, Kalitzeos A, Robson AG, u. a. Early Patterns of Macular Degeneration in ABCA4 -Associated Retinopathy. Ophthalmology. Mai 2018;125(5):735–46.

43. Lee W, Nõupuu K, Oll M, Duncker T, Burke T, Zernant J, u. a. The External Limiting Membrane in Early-Onset Stargardt Disease. Invest Ophthalmol Vis Sci. 2. Oktober 2014;55(10):6139.

44. Bax NM, Valkenburg D, Lambertus S, Klevering BJ, Boon CJF, Holz FG, u. a. Foveal Sparing in Central Retinal Dystrophies. Invest Ophthalmol Vis Sci. 9. August 2019;60(10):3456.

45. Chen L, Lee W, de Carvalho JRL, Chang S, Tsang SH, Allikmets R, u. a. Multi-platform imaging in ABCA4-Associated Disease. Sci Rep. 23. April 2019;9(1):6436.

46. Cideciyan AV, Swider M, Schwartz SB, Stone EM, Jacobson SG. Predicting Progression of ABCA4-Associated Retinal Degenerations Based on Longitudinal Measurements of the Leading Disease Front. Invest Ophthalmol Vis Sci. September 2015;56(10):5946–55.

47. Lopez PF, Maumenee IH, de la Cruz Z, Green WR. Autosomal-dominant fundus flavimaculatus. Clinicopathologic correlation. Ophthalmology. Juni 1990;97(6):798–809.

48. Sparrow JR, Marsiglia M, Allikmets R, Tsang S, Lee W, Duncker T, u. a. Flecks in Recessive Stargardt Disease: Short-Wavelength Autofluorescence, Near-Infrared Autofluorescence, and Optical Coherence Tomography. Invest Ophthalmol Vis Sci. 30. Juli 2015;56(8):5029.

49. Michaelides M, Chen LL, Brantley MA, Andorf JL, Isaak EM, Jenkins SA, u. a. ABCA4 mutations and discordant ABCA4 alleles in patients and siblings with bull's-eye maculopathy. British Journal of Ophthalmology. 1. Dezember 2007;91(12):1650–5.

50. Gupta MP, Herzlich AA, Sauer T, Chan CC. Retinal Anatomy and Pathology. In: Nguyen QD, Rodrigues EB, Farah ME, Mieler WF, Do DV, Herausgeber. Developments in Ophthalmology [Internet]. S. Karger AG; 2016 [zitiert 20. August 2023]. S. 7–17. Verfügbar unter: https://www.karger.com/Article/FullText/431128

51. Masland RH. The fundamental plan of the retina. Nat Neurosci. September 2001;4(9):877–86.

52. Wassle H, Boycott BB. Functional architecture of the mammalian retina. Physiological Reviews. 1. April 1991;71(2):447–80.

53. Staurenghi G, Sadda S, Chakravarthy U, Spaide RF, International Nomenclature for Optical Coherence Tomography (IN•OCT) Panel. Proposed lexicon for anatomic landmarks in normal posterior segment spectral-domain optical coherence tomography: the IN•OCT consensus. Ophthalmology. August 2014;121(8):1572–8.

54. Cideciyan AV, Aleman TS, Swider M, Schwartz SB, Steinberg JD, Brucker AJ, u. a. Mutations in ABCA4 result in accumulation of lipofuscin before slowing of the retinoid cycle: a reappraisal of the human disease sequence. Hum Mol Genet. 1. März 2004;13(5):525–34.

55. Spaide RF, Koizumi H, Pozonni MC. Enhanced Depth Imaging Spectral-Domain Optical Coherence Tomography. American Journal of Ophthalmology. Oktober 2008;146(4):496–500.

56. Han IC, Jaffe GJ. Comparison of Spectral- and Time-Domain Optical Coherence Tomography for Retinal Thickness Measurements in Healthy and Diseased Eyes. American Journal of Ophthalmology. Mai 2009;147(5):847-858.e1.

57. Menke MN, Dabov S, Knecht P, Sturm V. Reproducibility of retinal thickness measurements in patients with age-related macular degeneration using 3D Fourier-domain optical coherence tomography (OCT) (Topcon 3D-OCT 1000). Acta Ophthalmologica. Juni 2011;89(4):346–51.

58. Wolf-Schnurrbusch UEK, Ceklic L, Brinkmann CK, Iliev ME, Frey M, Rothenbuehler SP, u. a. Macular Thickness Measurements in Healthy Eyes Using Six Different Optical Coherence Tomography Instruments. Invest Ophthalmol Vis Sci. 1. Juli 2009;50(7):3432.

59. Wenner Y, Wismann S, Jäger M, Pons-Kühnemann J, Lorenz B. Interchangeability of macular thickness measurements between different volumetric protocols of Spectralis optical coherence tomography in normal eyes. Graefes Arch Clin Exp Ophthalmol. August 2011;249(8):1137–45.

60. Ibrahim MA, Sepah YJ, Symons RCA, Channa R, Hatef E, Khwaja A, u. a. Spectral- and time-domain optical coherence tomography measurements of macular thickness in normal eyes and in eyes with diabetic macular edema. Eye. März 2012;26(3):454–62.

61. Fujinami K, Singh R, Carroll J, Zernant J, Allikmets R, Michaelides M, u. a. Fine central macular dots associated with childhood-onset Stargardt Disease. Acta Ophthalmologica. März 2014;92(2):e157–9.

62. Hoon M, Okawa H, Della Santina L, Wong ROL. Functional architecture of the retina: Development and disease. Progress in Retinal and Eye Research. September 2014;42:44–84.

63. Carter-Dawson LD, Lavail MM. Rods and cones in the mouse retina. I. Structural analysis using light and electron microscopy. J Comp Neurol. 15. November 1979;188(2):245–62.

64. Delori FC, Dorey CK, Staurenghi G, Arend O, Goger DG, Weiter JJ. In vivo fluorescence of the ocular fundus exhibits retinal pigment epithelium lipofuscin characteristics. Invest Ophthalmol Vis Sci. März 1995;36(3):718–29.

65. Pole C, Ameri H. Fundus Autofluorescence and Clinical Applications. J Ophthalmic Vis Res. 2021;16(3):432–61.

66. von Ruckmann A, Fitzke FW, Bird AC. Distribution of fundus autofluorescence with a scanning laser ophthalmoscope. British Journal of Ophthalmology. 1. Mai 1995;79(5):407–12.

67. Verdina T, H. Tsang S. Functional Analysis of Retinal Flecks in Stargardt Disease. J Clinic Experiment Ophthalmol [Internet]. 2012 [zitiert 30. September 2022];03(06). Verfügbar unter: https://www.omicsonline.org/functional-analysis-of-retinal-flecks-in-stargardt-disease-2155-9570.1000233.php?aid=7632

68. Kuehlewein L, Hariri AH, Ho A, Dustin L, Wolfson Y, Strauss RW, u. a. COMPARISON OF MANUAL AND SEMIAUTOMATED FUNDUS AUTOFLUORESCENCE ANALYSIS OF MACULAR ATROPHY IN STARGARDT DISEASE PHENOTYPE. Retina. Juni 2016;36(6):1216–21.

69. Strauss RW, Muñoz B, Ho A, Jha A, Michaelides M, Cideciyan AV, u. a. Progression of Stargardt Disease as Determined by Fundus Autofluorescence in the Retrospective Progression of Stargardt Disease Study (ProgStar Report No. 9). JAMA Ophthalmol. 1. November 2017;135(11):1232.

70. Strauss RW, Kong X, Ho A, Jha A, West S, Ip M, u. a. Progression of Stargardt Disease as Determined by Fundus Autofluorescence Over a 12-Month Period: ProgStar Report No. 11. JAMA Ophthalmol. 1. Oktober 2019;137(10):1134.

71. Lois N. Phenotypic Subtypes of Stargardt Macular Dystrophy–Fundus Flavimaculatus. Arch Ophthalmol. 1. März 2001;119(3):359.

72. Scoles D, Sulai YN, Langlo CS, Fishman GA, Curcio CA, Carroll J, u. a. In Vivo Imaging of Human Cone Photoreceptor Inner Segments. Invest Ophthalmol Vis Sci. 11. Juli 2014;55(7):4244.

73. Song H, Rossi EA, Latchney L, Bessette A, Stone E, Hunter JJ, u. a. Cone and Rod Loss in Stargardt Disease Revealed by Adaptive Optics Scanning Light Ophthalmoscopy. JAMA Ophthalmol. 1. Oktober 2015;133(10):1198.

74. Russell S, Bennett J, Wellman JA, Chung DC, Yu ZF, Tillman A, u. a. Efficacy and safety of voretigene neparvovec (AAV2-hRPE65v2) in patients with RPE65 -mediated inherited

retinal dystrophy: a randomised, controlled, open-label, phase 3 trial. The Lancet. August 2017;390(10097):849–60.

75. Xue K, Jolly JK, Barnard AR, Rudenko A, Salvetti AP, Patrício MI, u. a. Beneficial effects on vision in patients undergoing retinal gene therapy for choroideremia. Nat Med. Oktober 2018;24(10):1507–12.

76. Cehajic-Kapetanovic J, Xue K, Martinez-Fernandez De La Camara C, Nanda A, Davies A, Wood LJ, u. a. Initial results from a first-in-human gene therapy trial on X-linked retinitis pigmentosa caused by mutations in RPGR. Nat Med. März 2020;26(3):354–9.

77. Grieger JC, Samulski RJ. Packaging Capacity of Adeno-Associated Virus Serotypes: Impact of Larger Genomes on Infectivity and Postentry Steps. J Virol. August 2005;79(15):9933–44.

78. Kantor A, McClements ME, Peddle CF, Fry LE, Salman A, Cehajic-Kapetanovic J, u. a. CRISPR genome engineering for retinal diseases. In: Progress in Molecular Biology and Translational Science [Internet]. Elsevier; 2021 [zitiert 20. August 2023]. S. 29–79. Verfügbar unter: https://linkinghub.elsevier.com/retrieve/pii/S1877117321000351

79. Peddle CF, Fry LE, McClements ME, MacLaren RE. CRISPR Interference–Potential Application in Retinal Disease. IJMS. 27. März 2020;21(7):2329.

80. Quinn J, Musa A, Kantor A, McClements ME, Cehajic-Kapetanovic J, MacLaren RE, u. a. Genome-Editing Strategies for Treating Human Retinal Degenerations. Human Gene Therapy. 1. März 2021;32(5–6):247–59.

81. Dellett M, Sasai N, Nishide K, Becker S, Papadaki V, Limb GA, u. a. Genetic Background and Light-Dependent Progression of Photoreceptor Cell Degeneration in Prominin-1 Knockout Mice. Investigative Ophthalmology & Visual Science. 9. Januar 2015;56(1):164–76.

82. Strauss RW, Muñoz B, Ahmed MI, Bittencourt M, Schönbach EM, Michaelides M, u. a. The Progression of the Stargardt Disease Type 4 (ProgStar-4) Study: Design and Baseline Characteristics (ProgStar-4 Report No. 1). Ophthalmic Res. 2018;60(3):185–94.

83. Csaky K, Ferris F, Chew EY, Nair P, Cheetham JK, Duncan JL. Report From the NEI/FDA Endpoints Workshop on Age-Related Macular Degeneration and Inherited Retinal Diseases. Invest Ophthalmol Vis Sci. 21. Juli 2017;58(9):3456.

84. World Medical Association Declaration of Helsinki: Ethical Principles for Medical Research Involving Human Subjects. JAMA. 27. November 2013;310(20):2191.

85. Velaga SB, Nittala MG, Jenkins D, Melendez J, Ho A, Strauss RW, u. a. Impact of segmentation density on spectral domain optical coherence tomography assessment in Stargardt disease. Graefes Arch Clin Exp Ophthalmol. März 2019;257(3):549–56.

86. Birch DG, Locke KG, Felius J, Klein M, Wheaton DKH, Hoffman DR, u. a. Rates of Decline in Regions of the Visual Field Defined by Frequency-Domain Optical Coherence

Tomography in Patients with RPGR-Mediated X-Linked Retinitis Pigmentosa. Ophthalmology. April 2015;122(4):833–9.

87. Strauss RW, Ho A, Muñoz B, Cideciyan AV, Sahel JA, Sunness JS, u. a. The Natural History of the Progression of Atrophy Secondary to Stargardt Disease (ProgStar) Studies. Ophthalmology. April 2016;123(4):817–28.

88. Testa F, Melillo P, Di Iorio V, Orrico A, Attanasio M, Rossi S, u. a. Macular Function and Morphologic Features in Juvenile Stargardt Disease. Ophthalmology. Dezember 2014;121(12):2399–405.

89. Testa F, Rossi S, Sodi A, Passerini I, Di Iorio V, Corte MD, u. a. Correlation between Photoreceptor Layer Integrity and Visual Function in Patients with Stargardt Disease: Implications for Gene Therapy. Invest Ophthalmol Vis Sci. 3. Juli 2012;53(8):4409.

90. Arepalli S, Traboulsi EI, Ehlers JP. ELLIPSOID ZONE MAPPING AND OUTER RETINAL ASSESSMENT IN STARGARDT DISEASE. Retina. Juli 2018;38(7):1427–31.

91. von Rückmann A, Fitzke FW, Bird AC. Fundus autofluorescence in age-related macular disease imaged with a laser scanning ophthalmoscope. Invest Ophthalmol Vis Sci. Februar 1997;38(2):478–86.

92. Wing GL, Blanchard GC, Weiter JJ. The topography and age relationship of lipofuscin concentration in the retinal pigment epithelium. Invest Ophthalmol Vis Sci. Juli 1978;17(7):601–7.

93. Gliem M, Müller PL, Birtel J, Herrmann P, McGuinness MB, Holz FG, u. a. Quantitative Fundus Autofluorescence and Genetic Associations in Macular, Cone, and Cone–Rod Dystrophies. Ophthalmology Retina. Juli 2020;4(7):737–49.

94. Mishra Z, Wang Z, Sadda SR, Hu Z. Automatic Segmentation in Multiple OCT Layers For Stargardt Disease Characterization Via Deep Learning. Trans Vis Sci Tech. 21. April 2021;10(4):24.

95. Kong X, Ho A, Munoz B, West S, Strauss RW, Jha A, u. a. Reproducibility of Measurements of Retinal Structural Parameters Using Optical Coherence Tomography in Stargardt Disease. Trans Vis Sci Tech. 21. Juni 2019;8(3):46.

96. Feuer WJ, Yehoshua Z, Gregori G, Penha FM, Chew EY, Ferris FL, u. a. Square Root Transformation of Geographic Atrophy Area Measurements to Eliminate Dependence of Growth Rates on Baseline Lesion Measurements: A Reanalysis of Age-Related Eye Disease Study Report No. 26. JAMA Ophthalmol. 1. Januar 2013;131(1):110.

97. Tanna P, Georgiou M, Aboshiha J, Strauss RW, Kumaran N, Kalitzeos A, u. a. Cross-Sectional and Longitudinal Assessment of Retinal Sensitivity in Patients With Childhood-Onset Stargardt Disease. Trans Vis Sci Tech. 27. November 2018;7(6):10.

98. Palejwala NV, Gale MJ, Clark RF, Schlechter C, Weleber RG, Pennesi ME. INSIGHTS INTO AUTOSOMAL DOMINANT STARGARDT-LIKE MACULAR DYSTROPHY

THROUGH MULTIMODALITY DIAGNOSTIC IMAGING. Retina. Januar 2016;36(1):119–30.

99. Garrity ST, Sarraf D, Freund KB, Sadda SR. Multimodal Imaging of Nonneovascular Age-Related Macular Degeneration. Invest Ophthalmol Vis Sci. 19. Juni 2018;59(4):AMD48.

100. Strauss RW, Muñoz B, Wolfson Y, Sophie R, Fletcher E, Bittencourt MG, u. a. Assessment of estimated retinal atrophy progression in Stargardt macular dystrophy using spectral-domain optical coherence tomography. British Journal of Ophthalmology. 1. Juli 2016;100(7):956–62.

101. Schönbach EM, Strauss RW, Kong X, Muñoz B, Ibrahim MA, Sunness JS, u. a. Longitudinal Changes of Fixation Location and Stability Within 12 Months in Stargardt Disease: ProgStar Report No. 12. American Journal of Ophthalmology. September 2018;193:54–61.

102. Strauss R, Muñoz B, Jha A, Ho A, Cideciyan A, Kasilian M, u. a. Comparison of Short-Wavelength Reduced-Illuminance and Conventional Autofluorescence Imaging in Stargardt Macular Dystrophy. American journal of ophthalmology. 10. Juni 2016;168.

103. Schließleder G, Kalitzeos A, Kasilian M, Singh N, Wang Z, Hu Z, u. a. Deep phenotyping of PROM1-associated retinal degeneration. Br J Ophthalmol. 20. April 2023;bjo-2022-322036.

104. Scholl HPN, Strauss RW, Singh MS, Dalkara D, Roska B, Picaud S, u. a. Emerging therapies for inherited retinal degeneration. Sci Transl Med [Internet]. 7. Dezember 2016 [zitiert 8. Mai 2022];8(368). Verfügbar unter: https://www.science.org/doi/10.1126/scitranslmed.aaf2838

105. Strauss RW, Kong X, Bittencourt MG, Ho A, Jha A, Schönbach EM, u. a. Scotopic Microperimetric Assessment of Rod Function in Stargardt Disease (SMART) Study: Design and Baseline Characteristics (Report No. 1). Ophthalmic Res. 2019;61(1):36–43.